

Current asymmetry and its implications for morphological changes in Vembanad Lake, the second largest wetland ecosystem in India

Sebin John¹², Revichandran C¹, Muraleedharan K.R*¹, Srijith B¹, Seena G¹², Abdul Azeez S¹.

¹CSIR-National Institute of Oceanography, Regional Centre, Kochi.

²Research Scholar, Bharathidasan University, Tiruchirappalli

*muraleedharan@nio.org

Abstract

Flow dynamics are a key part of the physical processes that drive the sediment transport in an aquatic system, affecting depositional processes and leading to landform evolution. The current asymmetry (CA) noted in Vembanad Lake (VL), India, have a particularly strong influence on the sediment budget and thus shape its geomorphology. In the present study the Coastal Ocean Model - Finite Volume Coastal Ocean Model (FVCOM) was used to compute the lateral current asymmetries and their implications for the long-term morphological changes in VL during different tidal phases. Model results were utilised to calculate the CA using two criteria: (1) Peak flood/ebb velocities with duration, and (2) Asymmetry Index (AI_{DV}). AI_{DV} values suggest the prevalence of ebb dominance over the entire system except at Cherai and Vallarpadam. However, several isolated pockets were noted on the right/eastern bank (shallow depth) of the system where the peak flood velocity exceeded the ebb, favouring accretion.

Contrary to the concept of ebb asymmetry, mean velocity and duration asymmetries were prevalent in the asymmetry index (AI_{DV}); hence we adopted peak flood/ebb velocity and its duration asymmetries to improve our understanding of the sediment transport dynamics. Typical flood asymmetry was identified on the right bank and at many of the lateral stations in VL, which switched to the modified ebb asymmetry during substantial river discharge. Analysis of CA enables understanding of the process that influences selective morphological changes, as explained by the model results. This conclusion was well corroborated by results obtained over the past three decades (1973-2008) from analysis of Landsat satellite imagery. Flood/ebb dominance in VL is explicitly substantiated with regions of accretion/erosion derived from satellite imageries. A holistic approach encompassing modelling, observations, remote sensing, and GIS techniques were used to address the erosion-accretion process in VL.

Keywords: ebb/flood dynamics, Current asymmetry, Morphology, FVCOM, Vembanad Lake, estuarine dynamics.

1 Introduction

The most heavily populated and generally the most important transition areas/ecotones on the coast are estuaries, tidal lakes, and deltas, where freshwater from river basins mixes with seawater to create the most biologically productive areas on earth (Levin et al., 2001). The buffer region between the permanent land and the sea is often inundated due to the action of tides, waves, and rivers in estuarine zones. However, future climate change has the potential to shift the buffer area (inundated zone) of estuarine systems inland. It is difficult to understand these transitions for any given estuary without detailed scientific analysis and process understanding. The key processes in an estuary are driven by the flow dynamics, which determine the water quality and the health of the ecosystem. At the same time, flow-induced transport of sediments controls landform evolution by depositional processes. Human activities, including the disruption of coastal development and sediment supply, have brought changes in estuaries around the world. These include a 65% loss of wetlands globally and a reduction in formerly important species of around 90% (Lotze et al., 2006). Furthermore, global sea level is accelerating to reach 0.3 to 1.2 m above its present level by 2100 (Kopp et al., 2014), which should be a key focus of future coastal development and planning. As a result, changes in sediment management practices in terms of source control and enhanced marsh accretion in tidal basins is expected. Therefore, residual transport of sediment during flood-ebb cycles is an important natural process that contributes to long term-morphological changes.

Tidal asymmetry is one of the most important processes governing residual sediment transport, causing large-scale morphological changes in tide-dominated systems such as estuaries, rivers, lakes, and lagoons (Gatto et al., 2017; Guo et al., 2016; Postma, 1961; Zhanhai et al., 2016). Tidal wave propagation towards the land may increase/decrease/remain constant depending upon relative changes in channel geometry, depth, bottom friction, and river discharge (Friedrichs and Aubrey, 1994; Jay, 1991; Lanzoni and Seminara, 1998; Nguyen et al., 2008; Prandle, 1985; Toffolon and Lanzoni, 2010). Internal and external processes in an estuary can induce tidal asymmetry. The asymmetry caused by the tidal distortion can be referred to as an internal process. Generally, these tidal distortions increase with estuarine length due to nonlinear interaction of higher harmonics (over tides and compound tides) in the tidal basin (Friedrichs and Madsen, 1992; Parker, 1991). In contrast, the asymmetry generated from different tidal constituents in the oceanic region at the seaward boundary of the estuary can be referred to as an external process. Numerous studies of tidal asymmetry have been conducted based on time series of water level and tides to provide detailed understanding of residual transport and long-term morphological changes (Guo et al., 2014; Lanzoni and Seminara, 2002; Speer and Aubrey, 1985). Flood currents dominate in estuaries with limited tidal flats and insignificant river discharges, while

ebb currents dominate in smaller estuaries with inter-tidal flats. The channels developed for navigation in ports and harbours also induce tidal asymmetry. When estuaries converge upstream, the systems are usually flood dominated. Large basins with different combinations of estuarine length and extent of tidal flats can be influenced by either flood or ebb dominance (Ridderinkhof et al., 2014).

The conventional definition of Current Asymmetry (CA) refers to the difference between the durations of rising and falling tides, as well as the difference in the duration and magnitude of flood and ebb currents (Speer et al., 1991). Thus, ebb dominance produces a stronger ebb current and a longer flood-tide duration, while flood dominance leads to a stronger flood current and a longer ebb-tide duration. The variation in peak velocity during flood-ebb durations determines the transport of bed material which is manifested in accretion or erosion. The difference in the durations of the flood-ebb currents is a proxy for the direction of net sediment due to the temporal settling lag, which is vital in fine sediment transport. Many researchers have highlighted the importance of tidal asymmetry in the transport and accumulation of sediments in various tidal systems including estuaries (Dronkers, 1986a; Friedrichs and Aubrey, 1988; Lanzoni and Seminara, 2002; Van de Kreeke and Robaczewska, 1993), tidal inlets (Aubrey and Friedrichs, 1988; Boon, 1988; Wang et al., 1995), and tidal basins (Postma, 1961; Ridderinkhof, 1988a, 1988b). Published data showing tidal asymmetry in the offshore region are also available (Aubrey, 1985; Dronkers, 1986b; Lessa and Masselink, 1995; Pingree et al., 1978; Pingree and Griffiths, 1979; Van de Kreeke and Robaczewska, 1993; Van der Molen, 2000). Ebb-dominated estuaries tend to export sediment in a seaward direction, whereas flood-dominated estuaries cause landward sediment transport (Allen et al., 1980; Dyer, 1997). The variation in the critical velocity due to flood-ebb asymmetry has a direct impact on the bed shear stress, thereby controlling the erosion and deposition (Mehta and Parchure, 2000; Tolhurst et al., 2000; Toublanc et al., 2015). Thus, knowledge of CA is essential to predict the geomorphological changes and stability of the estuary, which in turn is necessary to devise better management plans for dredging as well as for protecting estuarine habitats (Hunt et al., 2013).

Mixed semidiurnal regimes have received little attention in tidal asymmetries compared with semidiurnal estuarine systems. A few studies have highlighted the complexity of spatio-temporal variations in tidal asymmetry as this affects the sedimentation process (Daniell, 2015; Gong et al., 2016; Jewell et al., 2012; Nidzieko, 2010; Nidzieko and Ralston, 2012; O'Callaghan et al., 2010; Van Maren et al., 2004; Van Maren and Gerritsen, 2012). Most of these studies are concerned with tidal asymmetry in terms of the amplitude and phase lag in tidal elevations (phase relation of constituents, skewness of tidal elevations, etc.) and information regarding current asymmetry is somewhat limited. Vinita et al. (2015) analysed the skewness of the tidal elevation in Vembanad Lake (VL), India, and

showed that during low discharge the upstream region (shallow) of VL was flood dominated, while inlet and adjacent regions were ebb dominated. According to Revichandran et al. (2012), VL is completely flushed out from June to September (peak monsoon), moderately flushed from October to December (post-monsoon), not flushed at all between January and March (pre-monsoon). For a more complete understanding of the processes involved, current measurements are essential in the determination of the real asymmetry in VL, rather than the asymmetry inferred from the elevation alone. The tidal current is modified due to immense river discharge and enhanced ebb currents (Gallo and Vinzon, 2005; Horrevoets et al., 2004) and diminished flood currents through increased tidal friction (Godin, 1985; Sassi and Hoitink, 2013; Savenije, 2006). Quantitative estimation of long-term morphological changes in VL in terms of the natural and anthropogenic process was also undertaken (Gopalan et al., 1983; Kumar et al., 2013; Nair and Babu, 2016; Sreeshma and Vargheese, 2014). Kumar et al. (2013) revealed that long-term morphological changes were found to be characterised by strong progradation from 1967-2011. However, the relationship between the physical variability and hydrodynamic response to the alteration of the lake geometry is not fully understood. Hence, detailed knowledge of the current asymmetry is required to evaluate the changes/ modifications to the geometry of the lake. In this study FVCOM was used to understand the spatio-temporal variation of flood-ebb dominance and current asymmetry in VL. The model results were found to be in good agreement with the erosion and deposition zones as identified by Landsat satellite imageries analysis.

2 Vembanad Lake

VL is the second-largest wetland ecosystem in India, encompassing an area of approximately 260 km², interspaced with numerous islands and networks of canals making the circulation and transport mechanisms very complex (Revichandran et al., 2012). VL (Fig1.1) is aligned parallel to the Arabian Sea over 96 km from Munambam to Alappuzha, and it is directly connected to the Arabian Sea through two inlets, one at Fort Kochi (450m wide, depth >15m) and the other at Munambam (250 m wide, depth >7m). The tide in the VL is mixed semidiurnal with a range of 1 m that progressively decreases upstream (Janardanan et al., 2015; Revichandran et al., 2012; Shivaprasad et al., 2013b, 2013a; Srinivas et al., 2003b, 2003a; Vinita et al., 2015). The narrow and sinusoid portion of the lake (0.1-1km) lies on the northern side (Fig.1.2) from Munambam to Fort Kochi (27 km), while the broader portion (4-5 km) extends to the south (upper reaches) from Thanneermukkom to Alappuzha (14.5 km). This system receives a substantial supply of freshwater (~22000 Mm³/yr.) annually from seven major rivers flowing from the Western Ghats (Fig.1.1) with discharge peaking in the summer monsoon (Revichandran et al., 2012). During the monsoon period, VL maintains a steady seaward flow that alters the magnitude and direction of the tidal currents. High river discharge during the monsoon period

dampens the tidal current, which in turn increases the phase lag between high water and high-water slack. During the monsoon period, VL becomes a freshwater-dominated system except near the inlet regions, while in the post-monsoon season, the river discharges become moderate; as a result the tidal energy propagates further upstream making the estuary partially mixed. In the pre-monsoon season, the minimum river discharge and maximum seawater incursion upstream creates well mixed and homogenous water column up to Thanneermukkom Barrage (Menon et al., 2000). The accretion and siltation modes governed by the hydrodynamic conditions have resulted in the shrinkage of VL over the long term. In previous studies, VL was also referred to as a bar-built estuary, lagoons, among other terms (Rao and Balasubramanian, 1996) and the natural bar has been continuously dredged to maintain shipping channel 12-16m, ever since the commissioning of Cochin Port in 1936.

3 Data & Methodology

3.1 In-situ Observations

3.1.1 Hydrographic observations

A month-long set of observations of water level and currents were conducted for VL from 20th September to 20th October 2009. Water levels were recorded at 10-minute intervals at six different locations (Fig.1.2) using a Seabird SBE- 26 plus water level recorder having an accuracy of 0.1 % of full-scale (Strain Gauge Pressure). Aanderaa RCM-9 current meters were used to record speed and direction at 10-minute intervals with an accuracy of $\pm 0.15 \text{ cms}^{-1}$; $\pm 2^\circ$. Surface currents were measured at Arookutty and Thanneermukkom, while surface and bottom currents were measured at Fort Kochi. Daily river discharge and sediment concentration (sand, silt and clay) data from the seven river gauge stations were available from the Central water commission, Government of India (Fig.1.1) and utilised for the study. The sediment concentration in the water column was measured using the 0.6 D method at each river gauge station. A detailed description of the sampling procedures was given in the handbook for hydro metrological observations, January 2017, Central water commission, Government of India.

3.1.2 Grain Size analysis

Grain size is one of the most important physical properties of sediments and can reveal information about the sediment source, transport history, and depositional regime. Seventy-five sediment samples were collected from VL during August 2013 to understand the lateral (Left, Centre, Right) distribution of grain size (refer to Fig.11 in which the black-hollow circle represents the sampling locations around VL). Among these twenty-four samples were collected from exact points from 9 cross-sections as mentioned in the CA analysis section (F_L - F_R , K_L - K_R , L_L - L_R , M_L - M_R , N_L - N_R , O_L - O_R & P_L - P_R). The

grain size of the sediment samples was analysed using the Malvern Master Sizer 2000 laser diffraction analyser with a measurement range of 0.2-2000 μm (Dapkunas et al., 2001). The sediment grain size $>63\mu\text{m}$ and $<63\mu\text{m}$ are considered as coarse and fine particles, respectively. The distribution of the sediment in VL was interpreted based on median grain size (D_{50} μm).

3.2 Modelling Approach

An unstructured triangular grid was used in the Finite-volume coastal ocean model (FVCOM, v. 4.1) for better representation of the sinuous estuarine channels and land boundaries (Chen et al., 2003). The model decomposed the primitive equations over unstructured triangular grids with spatial resolutions varying from 10 m to 600 m over 15479 nodes and 22520 elements with ten uniform sigma-coordinate levels in the vertical grid. The grid was generated with Gmsh (version 2.5) developed by Geuzaine and Remacle (2009). The bathymetry data for the model was digitised from the Inland Water Authority Plan Chart-2006 (IWAI, NW-3) using QGIS. The bottom roughness parameter was set to 0.035 with a minimum value of 0.015 for the model drag coefficient. The model was forced with tides and freshwater influx for one month from 21-09-2009 16:00:00 to 20-10-2009 00:00:00.

3.2.1 Validation

The reliability of a hydrodynamic model depends on the comparison of the predicted results with in-situ observations (Fig.1.2) and statistical parameters such as the Coefficient of Determination- R^2 , Root Mean Square Error and Index of agreement (d).

Willmott, (1981) proposed an approach using the Index of agreement (d) defined as

$$d = 1 - \frac{\sum_{i=1}^N (P_i - O_i)^2}{\sum_{i=1}^N (|P_i - \bar{O}| + |O_i - \bar{O}|)^2}$$

where P and O represent the predicted and observed values respectively, \bar{O} is temporal mean of O , and N is the size of the data set. Perfect agreement between model results and observations yields a skill value of one and complete disagreement gives a skill value of zero.

3.3 Asymmetry analysis

After the validation and calibration of the FVCOM model for VL, the model was forced with the one-year tide and climatological river discharge. The results (pre-monsoon – January to May, monsoon – June to September and post-monsoon – October to December) were subjected to detailed analysis to understand the role of geometry, bottom topography, and freshwater influx in the generation of asymmetry (Fig.2.1). Sixteen sections (Fig 1.3) were selected across the channel to understand the temporal variations in flood-asymmetry in VL. The depth-averaged velocities were extracted from

each section at three lateral stations, Left, Centre and Right. The east and west side of the lake are considered to be the left and right stations except at A_L-A_R and F_L-F_R . The south and north shores of A_L-A_R and F_L-F_R are considered to be left-right lateral stations, as the boundary of the lake faces the west-east direction. During the pre-monsoon period, tidal propagation is obstructed at the Thanneermukkom barrage constructed to prevent salt intrusion towards the upper reaches of the VL. Hence the asymmetry analysis during the pre-monsoon period was limited to Thanneermukkom (O-O'). Velocity components 'v' (north-comp) & 'u' (east-comp) components were subjected to detailed harmonic analysis using TASK 2000. For each tidal constituent, the amplitude and phase of the u and v components were used to plot respective tidal ellipse parameters following standard equations (Pugh, 1987). By convention, the phase of the tidal current is usually taken as the phase of the maximum current. Among semidiurnal and diurnal constituents, M2 contributed significantly to the amplitude and phase of the total tidal current; hence M2 was chosen to understand the coherent/incoherent flow (*refer to supplementary information*). The results obtained from numerical modelling were utilised to assess the impact of CA based on the Asymmetry index (AI_{DV}) and Peak flood/ebb velocities with duration in VL

3.3.1 Asymmetry Index (AI_{DV})

This is a dimensionless index based on parameters proposed by (Lincoln and Fitzgerald, 1988) and used to describe the asymmetries in tidal duration (A_D) and mean velocity (A_V) between ebb and flood periods (Garonce and Quaresma, 2014; Mantovanelli et al., 2004).

$$\text{i.e. } AI_{DV} = A_D + A_V$$

The duration asymmetry (A_D) is defined as the ratio between the difference in the time span of ebb (t_e) -flood (t_f) periods and the summation of the time span of ebb (t_e) -flood (t_f) periods.

$$A_D = \frac{t_e - t_f}{t_e + t_f}$$

The mean velocity asymmetry (A_V) is described as the ratio between the difference in the average velocity in the water column during the ebb (u_e) -flood (u_f) and the sum of the average ebb (u_e) and flood (u_f) velocities.

$$A_V = \frac{u_e - u_f}{u_e + u_f}$$

Here, t_e & t_f are the duration of the ebb and flood periods computed based on the direction on the velocity, and u_e & u_f are the mean longitudinal velocity during ebb and flood, respectively.

Thus, when:

$AI_{DV} = 0$, The tidal wave is symmetrical for time and velocity;

$AI_{DV} > 0$, The residual circulation and water transport are in the ebb direction;

$AI_{DV} < 0$, The residual circulation and water transport are in the flood direction;

3.3.2 Peak flood/ebb velocities with duration

Current asymmetry strongly depends on the magnitude and duration of flood-ebb currents. Brown and Davies, 2010 proposed two ratios to determine the flood-ebb dominance and corresponding sediment transport (1) the ratio of peak flood velocity to that of ebb (U_p) and (2) the ratio of the flood to ebb duration (T_d). Where $U_p > 1$ this indicates flood dominance, and $U_p < 1$ indicates ebb dominance. There is a distinct zonation in the estuary based on the ebb/flood dominance (Fig. 2.2), such that Zone-1 ($U_p > 1$ & $T_d < 1$) represents typical flood asymmetry with shorter duration and maximum currents in the flood; Zone-2 ($U_p > 1$ & $T_d > 1$) corresponds to longer duration and maximum velocity during the flood; Zone-3 has typical ebb asymmetry ($U_p < 1$ & $T_d > 1$) characterised by shorter duration and maximum currents in the ebb, and Zone- 4 is characterised by a longer duration and maximum velocity during the ebb. Zone-1 and Zone-3 can be considered flood and ebb dominated, respectively, according to the conventional definition of CA.

3.4 Demarcation of Erosion Accretion zones

Numerous studies have been conducted to demarcate the accretion and erosion zone of the estuaries and lakes mostly through the application of remote sensing and GIS (Alphan and Yilmaz, 2005; Chen et al., 2005; Ke et al., 2011; Mahmud et al., 2011; Zhang et al., 2009). Limited information is available on the long-term morphological changes concerning the physical variability and hydrodynamic response of VL. In the present study, spatial analysis of multi-resolution Landsat images with less than 10% of cloud cover (<http://earthexplorer.usgs.gov/>) for the years 1973 (Landsat 1 MSS, February 1973) and 2008 (Landsat 5 TM, December 2008) provided information regarding the accretion and erosion zones. Multi-temporal images were co-registered in the same coordinate system, and all the images were re-projected to a standard projection, UTM with WGS84 datum and zone 43 N with RMSE value < 0.5 pixels. The spatiotemporal changes of VL (1973-2008) were delineated using Normalized Difference Water Index (NDWI) (McFeeters, 1996), Normalized Difference Vegetation Index (NDVI) (Rouse Jr et al., 1974), and Modified Normalized Differential Water Index (MNDWI) (Tebbs et al., 2013). The erosion and accretion zones in VL could be identified by selecting a suitable index, which was calculated, analysed and classified independently (using image-specific thresholds). Finally, the generated maps were stacked to produce the erosion/accretion zones for the period 1973-2008, and these were compared with the zones where flood/ebb dominance was noted.

4 Results

4.1 Model Validation

4.1.1 Validation of tide

Comparison of the predicted tidal elevation against observed water level is shown in Fig. 3. The statistical significance (Warner et al., 2005; Willmott, 1981) of the model output with observed data is given in Table 1. Quantitative comparisons based on regression analyses (0.87) and index of agreement (average skill value 0.92) reveal the reliability of the model in predicting the lake dynamics. The maximum error of 0.07 m (lowest index agreement 0.85) was observed at Thanneermukkom, where the freshwater influx was higher. A pulse of large freshwater flow from the rivers (Pampa, Achankovil, Meenachil, Muvatupuzha and Manimala) can cause a change in the surface water elevation in this region. The possibility of the error in the predicted water level could be due to inadequate discharge data from many tributaries to the lake.

4.1.2 Validation of currents

Modelled currents strongly depend upon the bathymetry data, the geometry of the lake, and the forcing parameters, hence accurate prediction of current is more complicated than that of the water elevation. However, the phase of the current components should be in agreement with observed data. Comparison between modelled and observed currents (east and north component) at 3 stations showed a significant correlation with maximum (0.88) index of agreement at Arookutty and minimum (0.61) at Thanneermukkom (Fig. 4, Table 2). Bi-directional flow at Fort Kochi inlet during the flood period (seaward surface flow and upstream flow near the bed) is captured by the model very well, where the indexes of agreement with the observed data at surface and bottom are 0.81 and 0.80 respectively. (Detailed description of the VL-FVCOM model validation for the tides, currents and salinity is presented in the companion paper -John et al., 2020).

4.2 Flood-Ebb velocity characteristics

A maximum velocity (supplementary Fig.2) was observed in Cochin inlet (F_L - F_R) with 0.77 m/s (pre-monsoon), 0.85 m/s (monsoon), 0.69 m/s (post-monsoon) during flood, with corresponding values during ebb of 0.68 m/s, 0.85 m/s and 0.80 m/s, respectively. At Munambam inlet (A_L - A_R) the maximum velocity in flood during pre-monsoon, monsoon and post-monsoon was 0.46 m/s, 0.37m/s, 0.2 m/s and in ebb 0.54 m/s, 0.57m/s, 0.47 m/s, respectively. In general to the south of Cochin inlet, there was a linear decrease in the current velocity irrespective of season and phase of the tide except for the cross-sections G_L - G_R , I_L - I_R and M_L - M_R . Owing to the shallow depth, the cross-sections G_L - G_R

and I_L - I_R sustained comparatively lower velocity both during flood and ebb. An abrupt increase at M_L - M_R was due to the funnelling effect. When the river discharge to VL was lowest during pre-monsoon, the tides overwhelmed the river discharge and controlled the flow dynamics. Strong flood currents were noted during the pre-monsoon compared to the other seasons. The difference between the peak flood and ebb velocities in the channel cross-sections are presented in Fig.5. The results reveal that more locations on the right/western bank (B, D, F, H, K, M, N) show stronger flood velocities than ebb during monsoon and post-monsoon. This implies that the system undergoes an effective interaction with the bottom geometry and incoming tides, leading to the formation of over-tides. During the monsoon and post-monsoon, increased freshwater influx dampens the tidal forcing, and intensifies the ebb flows through the eastern banks compared to that seen in the pre-monsoon period.

4.3 Assessment of spatial and temporal current asymmetry in VL

4.3.1 Asymmetry Index

AI_{DV} was calculated from asymmetries in duration (A_D) and mean velocity asymmetry (A_V) during the flood-ebb period, which was necessary for determining the net transport. Seasonal patterns of asymmetry index for VL are shown in Fig. 6 a, b and c. During the pre-monsoon (low discharge) period, the system exhibits a clear flood-ebb asymmetry index along the channel, while the duration asymmetry was higher during the monsoon and post-monsoon than during the pre-monsoon. This implies that the ebb duration is longer during the monsoon and post-monsoon periods. The right portion of the channel cross-section (F, G, H, K, M, N, O, and P) exhibits more flood dominance in A_V and the centre to the left portion of channel retains the ebb dominance during the pre-monsoon period. For the Asymmetry Index, the right side of the channel cross-section exhibits more flood dominance than the left and central portion of the channel in the pre-monsoon. However, the asymmetry pattern was entirely different in the monsoon and pre-monsoon period due to heavy discharge from the freshets. Time duration asymmetry in the monsoon and post-monsoon period were similar to those of the pre-monsoon period, but the magnitude of the duration was comparatively high. The average velocity asymmetry during the heavy and moderate discharge periods suggest a predominant ebb dominance in VL expect for cross-sections B, D, N, P during the monsoon and for C during the post-monsoon.

4.3.2 Flood-Ebb asymmetric ratio

In the present study, typical flood asymmetry (Zone-1) was identified on the right bank of VL; whereas characteristic ebb asymmetry was altogether absent in VL (Fig. 7 a, b and c). Flood and ebb asymmetric zones were more pronounced in the pre-monsoon season compared to the rest of the season. The

majority of the lateral stations in VL fall in Zone-4, which represents longer ebb duration and maximum ebb velocity during the pre-monsoon, monsoon and post-monsoon period. During the pre-monsoon (low discharge) period, modified ebb asymmetry prevailed at all stations as evidenced by the identical patterns (Fig.7 a.) for all lateral stations ($0.8 < T_d > 1$). The system switches from flood asymmetry to ebb asymmetry during pre-monsoon near to Cherai, B-B cross-section. This can be ascribed to the Periyar river influx, which influences the generation of flood asymmetry in the whole channel during the monsoon and post-monsoon period. Several consistent locations were identified with perennially flood dominated asymmetry on the right bank of VL (B, D, F, G, H, N), while the majority of the stations exhibited modified ebb asymmetry during the monsoon and post-monsoon period over a wide range of $0 < T_d > 1$. Taking a synoptic view of VL, it can be seen that the ebb velocities are higher on the left bank to the central axis of VL, while the flood currents dominate the other portion.

4.4 Demarcation of Erosion Accretion zones using satellite images

The erosion and accretion zones of VL over the period 1973-2008 were demarcated using remote sensing and GIS. A major shrinkage of the lake area was observed in regions adjacent to the Cochin inlet (Fig.8a), and most of this land ($\sim 4.62 \text{ km}^2$) was reclaimed for the construction of the marine drive, the extension of Willingdon Island, the construction of the railway track, and a road for the Vallarpadam Project International Container Trans-shipment Terminal, the Goshree project at Ernakulam jetty area, and the new Thevara -Willington Island bridge (Dipson et al., 2015). The northern part (Fig.8a) of the Cochin inlet region was found to protrude 1.6 km towards the sea with an area of 3.61 km^2 due to littoral drift along the coast. Comparatively fewer morphological alterations were observed in the southern part of the VL than the inlet region. Southern regions (southern half and upper reaches of the VL; refer to Fig 1.2 for locations) experienced natural accretion (3.51 km^2) and erosion (1.41 km^2) on the right and left banks, respectively. The analysis shows (Figs.7 and 8) that the major accretion zones were on the eastern bank ($D_R, E_R, F_R, H_R, I_R, J_R, K_R, L_R, M_R, N_R, O_R, P_R, P_L$) and the major erosion zones on the western boundary of the lake ($D_L, E_L, F_L, G_L, H_L, I_L, J_L, K_L, M_L, O_L$) as highlighted in the figures.

4.5 Sediment characteristics of Vembanad Lake.

In the previous section, we discussed the long-term morphological changes in VL and its association with the prevailing velocity asymmetry. Estimation of sediment flux from the rivers basin to the estuary is essential in order to understand the process of sediment mobility, transport, deposition, and erosion. Based on the climatological (2000-2016) analysis of sediment influx, the average annual yield of sediment from all the rivers draining into VL is calculated as $22 \times 10^5 \text{ t/yr}$ (Fig. 9). The maximum

sediment yield to VL was estimated during the monsoon (16.38×10^5 t), followed by post-monsoon (5.02×10^5 t) and pre-monsoon (0.85×10^5 t). Generally, a heterogeneous mixture of sediments flows through the rivers, and natural sorting takes place within the movement due to the different transport modes of fine and coarse materials. Fine fractions of the particles (clay) are transported in both low and high energy environments, while coarser particles are only transported under high energy environments of the rivers. Climatological analysis (2000-2016) of the sediment influx data from the seven rivers revealed that the contribution of clay particles (Fig.10.1 & 10.2) was significant during pre-monsoon (2-10 mg/l), monsoon (5-40 mg/l) and post-monsoon (4-45 mg/l). However, the rates of silt (3.27×10^5 t/yr.) and sand (1.37×10^5 t/yr.) transport were relatively low.

Even though the sediment contributions from the rivers were meagre during the pre-monsoon, the long (90 day) residence time (John et al., 2020) plays a significant role in depositing it in the upstream regions. Nevertheless, the contribution of sediment during the monsoon and post-monsoon is capable of exporting to the downstream parts of VL when the residence time is much shorter (25 days) compared to the pre-monsoon. The contribution of sand, silt and clay (mg/l) were found to be higher in the Achankovil River, while the discharge ($< 50 \text{ m}^3/\text{s}$) was significantly lower than in the other six rivers. Therefore, the contribution of sediment input to VL becomes minimal from the Achankovil River. The significant portion of the sediment to VL is contributed by the rivers Periyar and Muvatupuzha due to the higher discharge and high sediment load.

Sediment characteristics may be subject to changes during the transport processes in VL, and segregation is possible according to size, shape, mineralogy, and density (Oyedotun, 2016). Grain size data from VL (Fig. 11) shows the spatial distribution of sedimentation patterns with coarser particles ($> 400 \mu\text{m}$) near the Cochin inlet (by tidal action and littoral drift) and upstream regions (southern half and upper reaches). High settling velocities were noted for the rivers Muvattupuzha (southern half), and Meenachil, Manimala, Pamba and Achankovil (upper reaches), which favoured the deposition of coarser sediments in the southern part of VL. The spatial distribution of sediment showed coarser particles ($>150 \mu\text{m}$) deposited in the left/eastern bank and finer particles ($<150 \mu\text{m}$) on the right/western bank of VL. It is well known that coarser sediments tend to be transported during high energy flow conditions, while finer sediments will settle in a low energy environment (Folk, 1966; Friedman, 1967, 1962; Moiola and Weiser, 1968). CA analysis revealed that the left/western banks of the southern region (southern half and upper reaches) were dominated by modified ebb asymmetry that promotes a steady uniform flow towards the sea, limiting the settling of the fine fraction of the particles. This result corroborates the sediment grain size distribution seen in VL.

5 Discussion

CA analysis demonstrates the spatio-temporal variability (pre-monsoon, post-monsoon, monsoon) of the tidal asymmetry in VL. The asymmetry index delineates the distinct flood-ebb dominance in VL only for the pre-monsoon period, attributed to the substantial prevalence of tidal currents in the pre-monsoon compared with the other two seasons. During the monsoon and post-monsoon period, all the locations exhibited ebb dominance in the asymmetry index. This is because of the effect of peak flood on the average velocity by high fresher water influx to the system during the monsoon and post-monsoon period. However, in the case of flood-ebb asymmetry ratio, distinct flood-ebb dominance is observed in the monsoon and post-monsoon periods. Differential dominance over the channel cross-section shows that for particular cases, zones with maximum depth are characterised by ebb dominance and minimum depth zones by flood dominance. Hence, it may be concluded that the generating mechanism of CA is related not only to the interaction between the M_2 and M_4 tidal constituents but is also influenced by geometry, uneven topology, and freshwater influx to VL. These are explicitly illustrated by the flood-ebb asymmetry ratio proposed by Brown and Davies, 2010. In this study, it is evident that the residual flow becomes a predominant factor responsible for generating modified ebb asymmetry, which accounts for the effect of river discharge, bathymetry and geometry. Central water and power research station (2016) reported that the rate of siltation in the Ernakulam channel varied significantly between 2.3 – 3.2 m per year from 2010-2013 and more than 60% siltation occurred during monsoon periods. This also may be attributed to the river reinforced residual currents that interact with tidal currents and enhance the ebb currents thereby generating significant tidal residual sediment transport towards the sea (Guo et al., 2014). However, asymmetry analysis revealed that several isolated pockets on the eastern bank of VL attained flood dominance during all seasons. The magnitude of the velocity and the duration asymmetries between the flood/ebb periods significantly controls the net transport of dissolved and suspended material in VL. Thus CA is one of the most critical processes affecting residual sediment transport and associated large-scale morphological changes in tidal environments including estuaries, tidal inlets and lagoon systems, and coastal waters (De Swart and Zimmerman, 2009). Van de Kreeke and Robaczewska (1993) investigated the residual transport in the direction of the highest peak velocity in two cases, one for bedload transport (proportional to a power law of flow velocity) and other for suspended transport (proportional to the squared velocity via bed shear stress).

5.1 Significance of Current asymmetry in accretion and erosion in VL

Spatial velocity gradients largely control the process of erosion and deposition in the lake. John et al., 2020 revealed that maximum flushing occurs through the navigation channel (left bank) in the

southern part of VL. The spatial analyses demarcated the accretional zones on the right bank (minimum depth) and eroded zones on the left bank (maximum depth) of VL (Fig.8a, b, c & d). In the asymmetry index, VL exhibits ebb asymmetry during the monsoon and post-monsoon periods, but there is no great increase in the surface area of the lake between 1973-2008. This corroborates the findings of Bruun (1978) that 80% of the sediment transport takes place between 85% and 100% of the peak velocity. Therefore, the most significant current asymmetry in residual transport is the difference between the maximum current velocities occurring during the flood-ebb period, which controls the long-term morphological stability. Even though the asymmetry index depicts ebb dominance, the variation in the peak current velocity during the flood-ebb period has a significant role in residual transport in VL. Hence, at times the maximum velocity is higher during the flood than in the ebb (Fig.8) promoting deposition. At other times, the maximum velocity is higher during the ebb compared with the flood period promoting erosion.

This assumption is well supported by the heavy siltation (CWPRS 2016) noticed in the Cochin inlet, even though this region is under the influence of ebb asymmetry. Comparison of demarcated eroded/accreted zones (Fig.8) in VL with the ratio of peak flood-ebb velocity and its duration (Fig.5) revealed one-to-one correspondence identified with flood/ebb dominated zones in accreted/eroded zones. In accordance with peak flood-ebb velocity (Fig. 5), distinct channels were identified in several locations in VL; these were more vulnerable to deposition/erosion processes. Sustained flood dominance was identified on the right (B, F, H, M, N, O) and left banks (B, D, N, L) of VL. These regions showed flood dominance in the asymmetry analysis and are confirmed as accretional zones (Fig.8) through spatio-temporal satellite image analysis. Similarly, modified ebb asymmetry was identified on the left (E, F, G, H, I, J, K) and right (E, G, D) banks of VL; this is documented as eroded zones (Fig.8). From the above results, major anthropogenic encroachments in VL have primarily taken place in regions where a minimum flow velocity is observed. This is evident as a rapid alteration of the shoreline in the remote sensing data. It is worth mentioning that the flood dominated/accreting regions were invariably collocated with areas subject to decadal geomorphological changes on the eastern bank of VL. The modified ebb dominated/eroded regions are on the western bank of VL. The grain size distribution of sediments also revealed that coarse particles reside on the ebb dominated channel/western bank and finer particles reside on the flood dominated channel/eastern bank of VL (Fig.11), in good agreement with earlier reports by Sarkar et al., 2016; Veerayya and Murty, 1974. Due to channel orientation (orientation shifted from north-south to northwest-southeast), the flood-ebb channel is transposed in the meandering region L_L - L_R , resulting in sediment texture shifting westward to coarse particles and fine particles on the east side of VL.

From a global perspective, several studies have considered tidal asymmetry in estuaries, which confirm its importance in erosion and accretion processes. In a comparative analysis (Table.3 and Fig.12) of the flood/ebb dominance of the world estuaries, landward/seaward transport is found to be higher for coarse bed materials/suspended particles. Brown and Davies (2010) studied Dyfi estuary and elucidated the role of flood/ebb dominance in the relative extent of the channel and formation of sandbanks/flat. Nguyen et al.,(2008) identified the large scale of residual circulation between flood-ebb channels in the western Scheldt estuary. However, a nonlinear relationship was observed in the concentration of suspended particulate and flood-ebb velocities in Paranagua Bay (Mantovanelli et al., 2004). The suspended flux seen for ebb-dominated estuaries such as the Gironde estuary, Changjiang estuary and Johor estuary is net seawards and relatively higher during the ebb than the flood period (Castaing and Allen, 1981; Hasan et al., 2012; Zhanhai et al., 2016). Similarly, coarse bedload transport was relatively higher in the flood period than in the ebb in flood-dominated estuaries. In general, a shallow wider flood channel promotes landward transport/accretion, and a narrow deeper ebb channel maintains seaward transport/erosion, which clearly aligns with the findings of the present study. The existence of separate paths is maintained for peak ebb and flood velocities in Chesapeake Bay and hugs opposite shores for a meandering geometry. This similar pattern is also achieved in the present study in the strongly meandering regions of VL (L_L - L_R , N_L - N_R). Most of the regions in the VL experienced modified ebb asymmetry, and this feature was also found in the Dyfi and Charente estuary. Our own pioneering work to address the erosion-accretion process in Vembanad Lake based on current asymmetry combines modelling, observation, remote sensing & GIS techniques. The present study will pave the way for an integrated approach to address the sediment transport process in flood/ebb dominated estuaries around the world.

6 Conclusions

An open-source hydrodynamic model (FVCOM) was used to simulate the flow dynamics for understanding the spatial-temporal variation of flood-ebb dominance in VL. The reliability of the model was ascertained in terms of the Coefficient of determination (R^2), root mean square error and index of agreement. These skill measurements reveal that the model was well correlated with the observed water level (> 90%) and current data (>80%). This study has revealed the existence of flood-ebb asymmetries in VL, driven by the freshwater influx, geometry and bottom topography. AI_{DV} values suggest that ebb dominance prevailed over the entire system except at Cherai and Vallarpadam; however, there were several isolated pockets on the right bank of the system (shallow depth) where the peak flood velocity exceeds the ebb, favouring accretion. The region where the peak flood velocity exceeds the ebb was prone to accretion while the region where the peak ebb velocity exceeds the flood

was prone to erosion. The findings also lend credence to the morphological variation of VL over three decades (1973-2008) as identified by Landsat imagery of VL. Rapid Morphological changes can be attributed to anthropogenic alterations, while slow and steady changes are caused by natural processes. These slow and steady morphological changes in the VL are explicitly demonstrated in terms of Current asymmetry.

Acknowledgements

The authors thank Director, NIO, Goa, and Scientist-in-Charge, NIO, Cochin, for the encouragement and support. We are grateful to Dr A. C. Anil, Project Leader, OCEAN FINDER (PSC 0105) for financial support. We acknowledge ICMAM, Chennai (Ministry of Earth Sciences, India) and CSIR-NIO (Council of Scientific & Industrial Research, India) for the financial support to carry out this study. We want to thank the FVCOM development team members in the Marine Ecosystem Dynamics and Modeling Laboratory, School of Marine Science and Technology, UMASSD for providing FVCOM source code. We would also like to thank Dr Pierre W Cazenave, Plymouth Marine Laboratory, UK for the assistance and recommendation during the FVCOM installation and further setting of the model. We sincerely acknowledge Dr Priya K. Nair, english professor St. Teresa's College (an autonomous college under the Mahatma Gandhi University), Ernakulam, for proof editing of the manuscript. The fifth author thankfully acknowledge Department of Science and Technology (DST) -WOS-A scheme for research grant.

Author Contributions

Conceptualisation, M.K.R, S.J, and R.C; Modeling, S.J, M.K.R, AAS and S.B.; validation and formal analysis, M.K.R, S.J, AAS and S.G; writing—original draft preparation, S.J and M.K.R; writing—review and editing, R.C, A.A.S, S.G and S.B; Remote sensing and GIS, A.A.S and S.J; Supervision, R.C

Conflict of interest

The authors declare that they have no conflict of interest

References

- Ahnert, F., 1960. Estuarine meanders in the Chesapeake Bay area. *Geogr. Rev.* 50, 390–401.
- Allen, G.P., Salomon, J.C., Bassoullet, P., Du Penhoat, Y., De Grandpre, C., 1980. Effects of tides on mixing and suspended sediment transport in macrotidal estuaries. *Sediment. Geol.* 26, 69–90.
- Alphan, H., Yilmaz, K.T., 2005. Monitoring environmental changes in the Mediterranean coastal landscape: the case of Cukurova, Turkey. *Environ. Manage.* 35, 607–619.
- Aubrey, D.G., 1985. A Study of Nonlinear shallow Inlet / Estuarine Part I: Observations ” Tidal Propagation Systems in SC- M * 185–205.
- Aubrey, D.G., Friedrichs, C.T., 1988. Seasonal climatology of tidal non-linearities in a shallow estuary, in: *Hydrodynamics and Sediment Dynamics of Tidal Inlets*. Springer, pp. 103–124.
- Austin, T.P., Short, A.D., Hughes, M.G., Ranasinghe, R., 2009. Tidal Hydrodynamics of a Micro-tidal , Wave Dominated Flood-tide Delta : Port Stephens , Australia 2009, 693–697.
- Boon, J.D., 1988. Temporal variation of shallow-water tides in basin-inlet systems, in: *Hydrodynamics and Sediment Dynamics of Tidal Inlets*. Springer, pp. 125–136.
- Brown, J.M., Davies, A.G., 2010. Flood/ebb tidal asymmetry in a shallow sandy estuary and the impact on net sand transport. *Geomorphology* 114, 431–439.
- Bruun, P., 1978. *Stability of Tidal Inlets: Theory and Engineering, Volume 23 (Developments in Geotechnical Engineering)*.
- Castaing, P., Allen, G.P., 1981. Mechanisms controlling seaward escape of suspended sediment from the Gironde: a macrotidal estuary in France. *Mar. Geol.* 40, 101–118.
- Central water and power research station, pune, 2016. Mathematical model studies for assesing the effect of proposed new dry dock of Cochin shipyard on DPR- CSL NEW DRY DOCK - APPENDIX A1 C A1.
- Central water commision, government of India, January 2017. Handbook of hydrometeorological obervations.
- Chen, C., Liu, H., Beardsley, R.C., 2003. An unstructured grid, finite-volume, three-dimensional, primitive equations ocean model: application to coastal ocean and estuaries. *J. Atmos. Ocean. Technol.* 20, 159–186.
- Chen, S., Chen, L., Liu, Q., Li, X., Tan, Q., 2005. Remote sensing and GIS-based integrated analysis of coastal changes and their environmental impacts in Lingding Bay, Pearl River Estuary, South China. *Ocean Coast. Manag.* 48, 65–83.
- Daniell, J.J., 2015. Bedload parting in western Torres Strait, northern Australia. *Cont. Shelf Res.* 93, 58–69.
- Dapkunas, S.J., Jillavenkatesa, A., Lum, L.H., 2001. Particle Size Characterisation. NIST, Gaithersburg, MD.
- De Swart, H.E., Zimmerman, J.T.F., 2009. Morphodynamics of tidal inlet systems. *Annu. Rev. Fluid Mech.* 41, 203–229.
- Dipson, P.T., Chithra, S. V, Amarnath, A., Smitha, S. V, Nair, M.V.H., Shahin, A., 2015. Spatial changes of estuary in Ernakulam district, Southern India for last seven decades, using multi-temporal satellite data. *J. Environ. Manage.* 148, 134–142.
- Dronkers, J., 1986a. Tidal asymmetry and estuarine morphology. *Netherlands J. Sea Res.* 20, 117–131.

[https://doi.org/10.1016/0077-7579\(86\)90036-0](https://doi.org/10.1016/0077-7579(86)90036-0)

- Dronkers, J., 1986b. Tide-induced residual transport of fine sediment. *Phys. shallow estuaries bays* 16, 228–244.
- Dyer, K.R., 1997. *Estuaries: A physical introduction*, Wiley. New York 1.
- Folk, R.L., 1966. A review of grain-size parameters. *Sedimentology* 6, 73–93.
- Friedman, G.M., 1967. Dynamic processes and statistical parameters compared for size frequency distribution of beach and river sands. *J. Sediment. Res.* 37, 327–354.
- Friedman, G.M., 1962. On sorting, sorting coefficients, and the lognormality of the grain-size distribution of sandstones. *J. Geol.* 70, 737–753.
- Friedrichs, C.T., Aubrey, D.G., 1994. Tidal propagation in strongly convergent channels. *J. Geophys. Res. Ocean.* 99, 3321–3336.
- Friedrichs, C.T., Aubrey, D.G., 1988. Nonlinear tidal distortion in shallow well-mixed estuaries: a synthesis. *Estuar. Coast. Shelf Sci.* 27, 521–545.
- Friedrichs, C.T., Madsen, O.S., 1992. Nonlinear diffusion of the tidal signal in frictionally dominated embayments. *J. Geophys. Res. Ocean.* 97, 5637–5650.
- Gallo, M.N., Vinzon, S.B., 2005. Generation of overtides and compound tides in Amazon estuary. *Ocean Dyn.* 55, 441–448.
- Garonce, F.A.A., Quaresma, V.S., 2014. Hydrodynamic Aspects at Vitória Bay Mouth, ES. *An. Acad. Bras. Cienc.* 86, 555–570.
- Gatto, V.M., van Prooijen, B.C., Wang, Z.B., 2017. Net sediment transport in tidal basins: quantifying the tidal barotropic mechanisms in a unified framework. *Ocean Dyn.* 67, 1385–1406.
- Geuzaine, C., Remacle, J.-F., 2009. Gmsh: A 3-D finite element mesh generator with built-in pre-and post-processing facilities. *Int. J. Numer. Methods Eng.* 79, 1309–1331.
- Godin, G., 1985. Modification of river tides by the discharge. *J. Waterw. port, coastal, Ocean Eng.* 111, 257–274.
- Gong, W., Schuttelaars, H., Zhang, H., 2016. Tidal asymmetry in a funnel-shaped estuary with mixed semidiurnal tides. *Ocean Dyn.* 66, 637–658.
- Gopalan, U.K., Vengayil, D.T., Udayavarma, V.P., Krishnankutty, M., 1983. The shrinking backwaters of Kerala. *J. Mar. Biol. Assoc. India. Cochin* 25, 131–141.
- Guo, L., der Wegen, M., Roelvink, J.A., He, Q., 2014. The role of river flow and tidal asymmetry on 1-D estuarine morphodynamics. *J. Geophys. Res. Earth Surf.* 119, 2315–2334.
- Guo, W., Song, D., Wang, X.H., Ding, P., Ge, J., 2016. Contributions of different tidal interactions to fortnightly variation in tidal duration asymmetry. *J. Geophys. Res. Ocean.* 121, 5980–5994.
- Hasan, G.M.J., van Maren, D.S., Fatt, C.H., 2012. Numerical study on mixing and stratification in the ebb-dominant Johor Estuary. *J. Coast. Res.* 29, 201–215.
- Horrevoets, A.C., Savenije, H.H.G., Schuurman, J.N., Graas, S., 2004. The influence of river discharge on tidal damping in alluvial estuaries. *J. Hydrol.* 294, 213–228.

- Hunt, S., Bryan, K.R., Mullarney, J.C., Pritchard, M., 2013. The Control of Wind and Waves on the Asymmetry of Estuarine Currents, in: Coastal Dynamics 2013. pp. 859–870.
- Janardanan, V., Amaravayal, S., Revichandran, C., Manoj, N.T., Muraleedharan, K.R., Jacob, B., 2015. Salinity Response to Seasonal Runoff in a Complex Estuarine System (Cochin Estuary, West Coast of India). *J. Coast. Res.* 314. <https://doi.org/10.2112/JCOASTRES-D-13-00038.1>
- Jay, D.A., 1991. Green's law revisited: Tidal long-wave propagation in channels with strong topography. *J. Geophys. Res. Ocean.* 96, 20585–20598.
- Jewell, S.A., Walker, D.J., Fortunato, A.B., 2012. Tidal asymmetry in a coastal lagoon subject to a mixed tidal regime. *Geomorphology* 138, 171–180.
- John, S., Muraleedharan, K.R., Revichandran, C., Azeez, S.A., Seena, G., Cazenave, P.W., K.R., M., C., R., S., A.A., G., S., Cazenave, P.W., 2020. What Controls the Flushing Efficiency and Particle Transport Pathways in a Tropical Estuary? Cochin Estuary, Southwest Coast of India. *Water* 2020, Vol. 12, Page 908 12, 908. <https://doi.org/10.3390/W12030908>
- Ke, C.-Q., Zhang, D., Wang, F.-Q., Chen, S.-X., Schmullius, C., Boerner, W.-M., Wang, H., 2011. Analysing coastal wetland change in the Yancheng national nature reserve, China. *Reg. Environ. Chang.* 11, 161–173.
- Kopp, R.E., Horton, R.M., Little, C.M., Mitrovica, J.X., Oppenheimer, M., Rasmussen, D.J., Strauss, B.H., Tebaldi, C., 2014. Probabilistic 21st and 22nd century sea-level projections at a global network of tide-gauge sites. *Earth's Futur.* 2, 383–406.
- Kumar, P.K.D., Gopinath, G., Murali, R.M., Muraleedharan, K.R., 2013. Geospatial analysis of long-term morphological changes in Cochin estuary, SW coast of India. *J. Coast. Res.* 30, 1315–1320.
- Lanzoni, S., Seminara, G., 2002. Long-term evolution and morphodynamic equilibrium of tidal channels. *J. Geophys. Res. Ocean.* 107, 1.
- Lanzoni, S., Seminara, G., 1998. On tide propagation in convergent estuaries. *J. Geophys. Res. Ocean.* 103, 30793–30812.
- Lessa, G., Masselink, G., 1995. Morphodynamic evolution of a macrotidal barrier estuary. *Mar. Geol.* 129, 25–46. [https://doi.org/10.1016/0025-3227\(95\)00103-4](https://doi.org/10.1016/0025-3227(95)00103-4)
- Levin, L.A., Boesch, D.F., Covich, A., Dahm, C., Erséus, C., Ewel, K.C., Kneib, R.T., Moldenke, A., Palmer, M.A., Snelgrove, P., Strayer, D., Weslawski, J.M., 2001. The function of marine critical transition zone and the importance of sediment biodiversity. *Ecosystems* 4, 430–451.
- Lincoln, J.M., Fitzgerald, D.M., 1988. Tidal distortions and flood dominance at five small tidal inlets in southern Maine. *Mar. Geol.* 82, 133–148.
- Lotze, H.K., Lenihan, H.S., Bourque, B.J., Bradbury, R.H., Cooke, R.G., Kay, M.C., Kidwell, S.M., Kirby, M.X., Peterson, C.H., Jackson, J.B.C., 2006. Depletion, degradation, and recovery potential of estuaries and coastal seas. *Science* (80-.). 312, 1806–1809.
- Mahmud, M.S., Masrur, A., Ishtiaque, A., Haider, F., Habiba, U., 2011. Remote sensing & GIS based spatio-temporal change analysis of Wetland in Dhaka City, Bangladesh. *J. Water Resour. Prot.* 3, 781.
- Manoj, N.T., Unnikrishnan, A.S., Sundar, D., 2009. Tidal asymmetry in the Mandovi and Zuari estuaries, the west coast of India. *J. Coast. Res.* 1187–1197.

- Mantovanelli, A., Marone, E., Da Silva, E.T., Lautert, L.F., Klingenfuss, M.S., Prata, V.P., Noernberg, M.A., Knoppers, B.A., Angulo, R.J., 2004. Combined tidal velocity and duration asymmetries as a determinant of water transport and residual flow in Paranaguá Bay estuary. *Estuar. Coast. Shelf Sci.* 59, 523–537. <https://doi.org/10.1016/j.ecss.2003.09.001>
- McFeeters, S.K., 1996. The use of the Normalised Difference Water Index (NDWI) in the delineation of open water features. *Int. J. Remote Sens.* 17, 1425–1432.
- Mehta, A.J., Parchure, T.M., 2000. Surface erosion of fine-grained sediment revisited. *Proc. Mar. Sci.* 2, 55–74.
- Menon, N.N., Balchand, A.N., Menon, N.R., 2000. Hydrobiology of the Cochin backwater system - A review. *Hydrobiologia*. <https://doi.org/10.1023/A:1004033400255>
- Moiola, R.J., Weiser, D., 1968. Textural parameters; an evaluation. *J. Sediment. Res.* 38, 45–53.
- Nair, P.K., Babu, D.S.S., 2016. Spatial shrinkage of Vembanad Lake, south west India during 1973-2015 using NDWI and MNDWI. *Int. J. Sci. Res.* 5, 1394–1401.
- Nguyen, A.D., Savenije, H.H.G., van der Wegen, M., Roelvink, D., 2008. New analytical equation for dispersion in estuaries with a distinct ebb-flood channel system. *Estuar. Coast. Shelf Sci.* 79, 7–16.
- Nidzieko, N.J., 2010. Tidal asymmetry in estuaries with mixed semidiurnal/diurnal tides. *J. Geophys. Res. Ocean.* 115.
- Nidzieko, N.J., Ralston, D.K., 2012. Tidal asymmetry and velocity skew over tidal flats and shallow channels within a macrotidal river delta. *J. Geophys. Res. Ocean.* 117.
- O’Callaghan, J.M., Pattiaratchi, C.B., Hamilton, D.P., 2010. The role of intratidal oscillations in sediment resuspension in a diurnal, partially mixed estuary. *J. Geophys. Res. Ocean.* 115.
- Oyedotun, T.D.T., 2016. Sediment characterisation in an Estuary-beach system. *J Coast Zo. Manag* 19, 2.
- Parker, B.B., 1991. The relative importance of the various nonlinear mechanisms in a wide range of tidal interactions. *Tidal Hydrodyn.* Ed. by B. B. Park. 237–268.
- Pingree, R.D., Griffiths, D.K., 1979. Sand transport paths around the British Isles resulting from M 2 and M 4 tidal interactions. *J. Mar. Biol. Assoc. United Kingdom* 59, 497–513.
- Pingree, R.D., RD, P., others, 1978. The M4 tide in the English Channel derived from a nonlinear numerical model of the M2 tide.
- Postma, H., 1961. Transport and accumulation of suspended matter in the Dutch Wadden Sea. *Netherlands J. Sea Res.* 1, 148–190.
- Prandle, D., 1985. Classification of tidal response in estuaries from channel geometry. *Geophys. J. Int.* 80, 209–221.
- Pugh, D.T., 1987. *Tides, surges and mean sea-level: a handbook for engineers and scientists*, 472 pp.
- Rao, K.K., Balasubramanian, T., 1996. Distribution of foraminifera in the Cochin estuary.
- Revichandran, C., Srinivas, K., Muraleedharan, K.R., Rafeeq, M., Amaravayal, S., Vijayakumar, K., Jayalakshmy, K. V., 2012. Environmental set-up and tidal propagation in a tropical estuary with dual connection to the sea (SW Coast of India). *Environ. Earth Sci.* 66, 1031–1042. <https://doi.org/10.1007/s12665-011-1309-0>

- Ridderinkhof, H., 1988a. Tidal and residual flows in the Western Dutch Wadden Sea I: numerical model results. *Netherlands J. Sea Res.* 22, 1–21.
- Ridderinkhof, H., 1988b. Tidal and residual flows in the Western Dutch Wadden Sea II: an analytical model to study the constant flow between connected tidal basins. *Netherlands J. Sea Res.* 22, 185–198.
- Ridderinkhof, W., De Swart, H.E., Van Der Vegt, M., Alebregtse, N.C., Hoekstra, P., 2014. Geometry of tidal inlet systems: A key factor for the net sediment transport in tidal inlets. *J. Geophys. Res. Ocean.* <https://doi.org/10.1002/2014JC010226>
- Rouse Jr, J., Haas, R.H., Schell, J.A., Deering, D.W., 1974. Monitoring vegetation systems in the Great Plains with ERTS. *Proc. Third Earth Resour. Technol. Symp. Greenbelt, ON, Canada SP-351*, 309–317.
- Sarkar, A., Chakraborty, P., Nagender Nath, B., 2016. Distribution and nature of sedimentary organic matter in a tropical estuary: An indicator of human intervention on environment. *Mar. Pollut. Bull.* 102, 176–186. <https://doi.org/10.1016/j.marpolbul.2015.11.013>
- Sassi, M.G., Hoitink, A.J.F., 2013. River flow controls on tides and tide-mean water level profiles in a tidal freshwater river. *J. Geophys. Res. Ocean.* 118, 4139–4151.
- Savenije, H.H.G., 2006. *Salinity and tides in alluvial estuaries*. Elsevier.
- Shivaprasad, A., Vinita, J., Revichandran, C., Manoj, N.T., Jayalakshmy, K. V, Muraleedharan, K.R., 2013a. Ambiguities in the classification of Cochin estuary, West coast of India. *Hydrol. Earth Syst. Sci. Discuss.* 3595–3628.
- Shivaprasad, A., Vinita, J., Revichandran, C., Reny, P.D., Deepak, M.P., Muraleedharan, K.R., NaveenKumar, K.R., 2013b. Seasonal stratification and property distributions in a tropical estuary (Cochin estuary, west coast, India).
- Speer, P.E., Aubrey, D.G., 1985. A study of nonlinear tidal propagation in shallow inlet/estuarine systems Part II: Theory. *Estuar. Coast. Shelf Sci.* 21, 207–224.
- Speer, P. E., D. G. Aubrey, and C. T. Friedrichs (1991), Nonlinear hydrodynamics of shallow tidal inlet/estuary systems, in *Tidal Hydrodynamics*, edited by B. B. Parker, pp. 319–339, Wiley, New York
- Sreeshma, A., Vargheese, K.O., 2014. Long-Time Shoreline Monitoring of the Cochin Estuarine System, Southwest Coast of India Using Satellite Data. *Int. J. Sci. Eng. Res.* 5, 324–330.
- Srinivas, K., Revichandran, C., Maheswaran, P.A., Asharaf, T.T.M., Murukesh, N., 2003a. Propagation of tides in the Cochin estuarine system, southwest coast of India.
- Srinivas, K., Revichandran, C., Thottam, T.J., Maheswaran, P.A., Mohamed Asharaf, T.T., Murukesh, N., 2003b. Currents in the Cochin estuarine system [southwest coast of India] during March 2000. *Indian J. Mar. Sci.* 32, 123–132.
- Tebbs, E.J., Remedios, J.J., Avery, S.T., Harper, D.M., 2013. Remote sensing the hydrological variability of Tanzania's Lake Natron, a vital Lesser Flamingo breeding site under threat. *Ecohydrol. Hydrobiol.* 13, 148–158.
- Toffolon, M., Lanzoni, S., 2010. Morphological equilibrium of short channels dissecting the tidal flats of coastal lagoons. *J. Geophys. Res. Earth Surf.* 115.

- Tolhurst, T.J., Black, K.S., Paterson, D.M., Mitchener, H.J., Termaat, G.R., Shayler, S.A., 2000. A comparison and measurement standardisation of four in situ devices for determining the erosion shear stress of intertidal sediments. *Cont. Shelf Res.* 20, 1397–1418. [https://doi.org/10.1016/S0278-4343\(00\)00029-7](https://doi.org/10.1016/S0278-4343(00)00029-7)
- Toublanc, F., Brenon, I., Coulombier, T., Moine, O. Le, 2015. Fortnightly tidal asymmetry inversion and its impact on salinity distribution and sediment net transport in a shallow macrotidal estuary (Charente , France). *Cont. Shelf Res.* 94, 42–54. <https://doi.org/http://dx.doi.org/10.1016/j.csr.2014.12.009>
- Van de Kreeke, J., Robaczewska, K., 1993. Tide-induced residual transport of coarse sediment; application to the Ems estuary. *Netherlands J. Sea Res.* 31, 209–220.
- Van der Molen, J., 2000. A 2DH numerical model of tidally induced sand transport in the southern North Sea. *Interact. between estuaries Coast. seas shelf seas.* Terra Sci. Tokyo 265–285.
- Van Maren, D.S., Gerritsen, H., 2012. Residual flow and tidal asymmetry in the Singapore Strait, with implications for resuspension and residual transport of sediment. *J. Geophys. Res. Ocean.* 117.
- Van Maren, D.S., Hoekstra, P., Hoitink, A.J.F., 2004. Tidal flow asymmetry in the diurnal regime: bedload transport and morphologic changes around the Red River Delta. *Ocean Dyn.* 54, 424–434.
- Veerayya, M., Murty, P.S.N., 1974. Studies on the sediments of Vembanad Lake, Kerala state: Part III-distribution and interpretation of bottom sediments. *Indian J. Mar. Sci.* 3, 16–27.
- Vinita, J., Shivaprasad, A., Manoj, N.T., Revichandran, C., 2015. Spatial tidal asymmetry of Cochin estuary , West Coast , India 537–551. <https://doi.org/10.1007/s11852-015-0405-9>
- Wang, Y.-H., Ridd, P. V, Wu, H.-L., Wu, J.-X., Shen, H.-T., 2008. Long-term morphodynamic evolution and the equilibrium mechanism of a flood channel in the Yangtze Estuary (China). *Geomorphology* 99, 130–138.
- Wang, Z.B., Louters, T., de Vriend, H.J., 1995. Morphodynamic modelling for a tidal inlet in the Wadden Sea. *Mar. Geol.* 126, 289–300.
- Warner, J.C., Geyer, W.R., Lerczak, J.A., 2005. Numerical modeling of an estuary: A comprehensive skill assessment. *J. Geophys. Res. Ocean.* 110.
- Willmott, C.J., 1981. On the validation of models. *Phys. Geogr.* 2, 184–194.
- Zhang, S., Na, X., Kong, B., Wang, Z., Jiang, H., Yu, H., Zhao, Z., Li, X., Liu, C., Dale, P., 2009. Identifying Wetland Change in China's Sanjiang Plain Using Remote Sensing. *Wetlands* 29. <https://doi.org/10.1672/08-04.1>
- Zhanhai, L.I., Yaping, W., Peng, C., Guoan, Z., Jiufa, L.I., 2016. Flood-ebb asymmetry in current velocity and suspended sediment transport in the Changjiang Estuary 35, 37–47. <https://doi.org/10.1007/s13131-016-0923-9>

Figures:

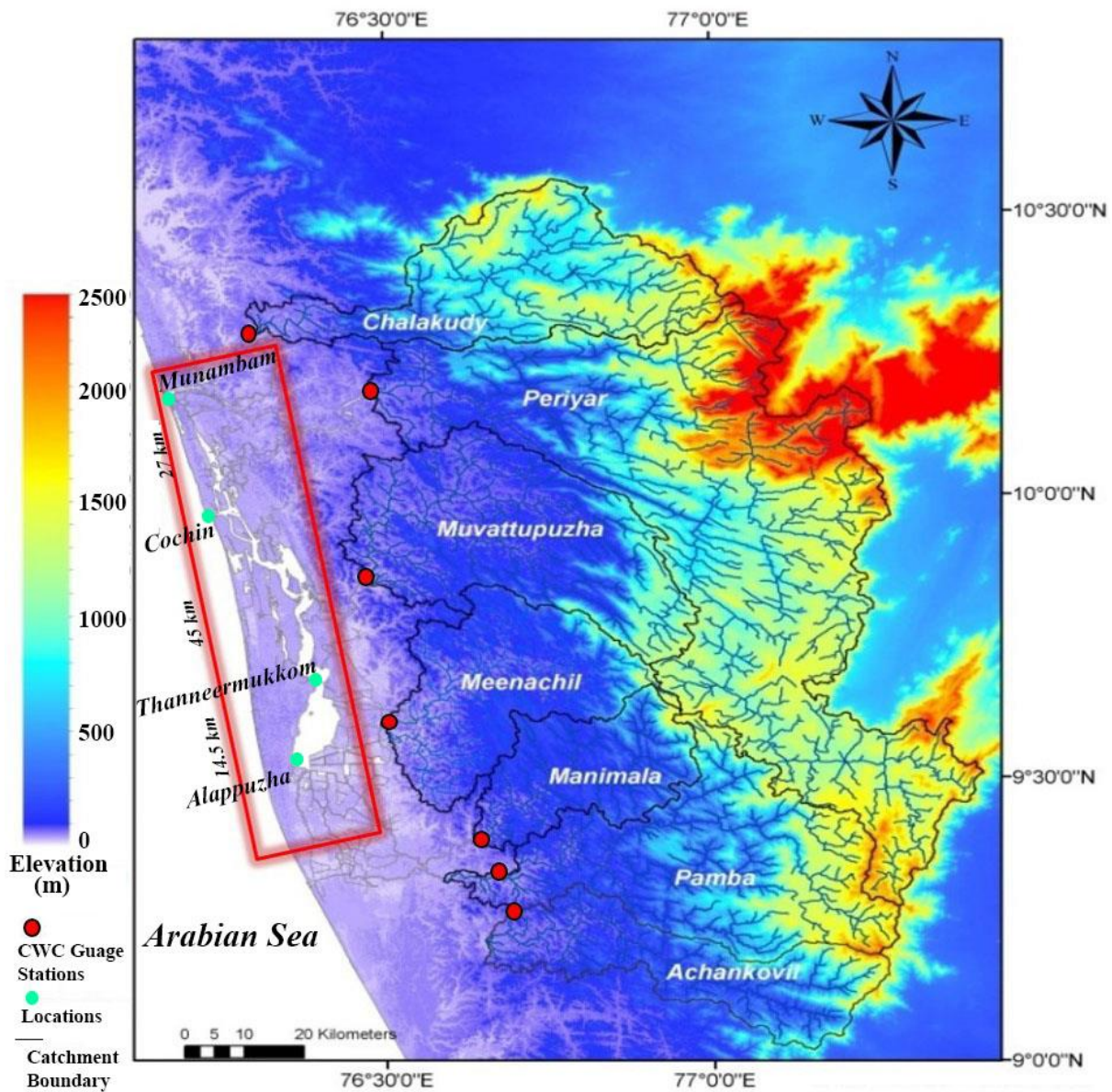


Fig. 1.1 Digital elevation (The Shuttle Radar Topography Mission (SRTM) - 90-meter resolution data) map shows model domain (red box), Central Water Commission river gauge stations (red dots), Major locations in the VL (cyan dots) and River Catchment boundaries (black line). Numerous rivulets join to stream and then rivers in the catchment area of each river can be seen in the map.

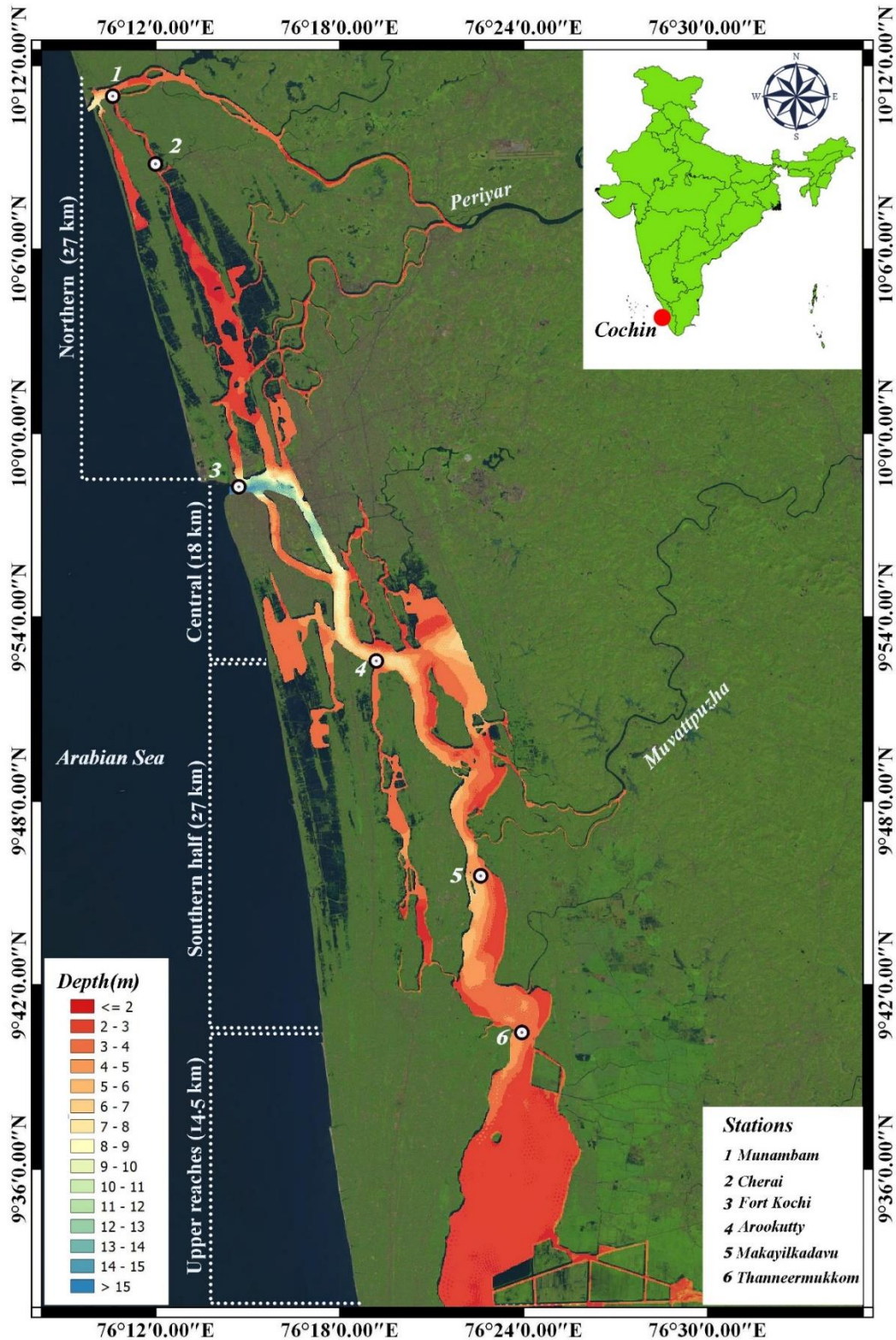


Fig. 1.2. Vembanad lake map shows the model domain over the satellite image with interpolated bathymetry and marked the observation locations for model validation (Tides & Currents).

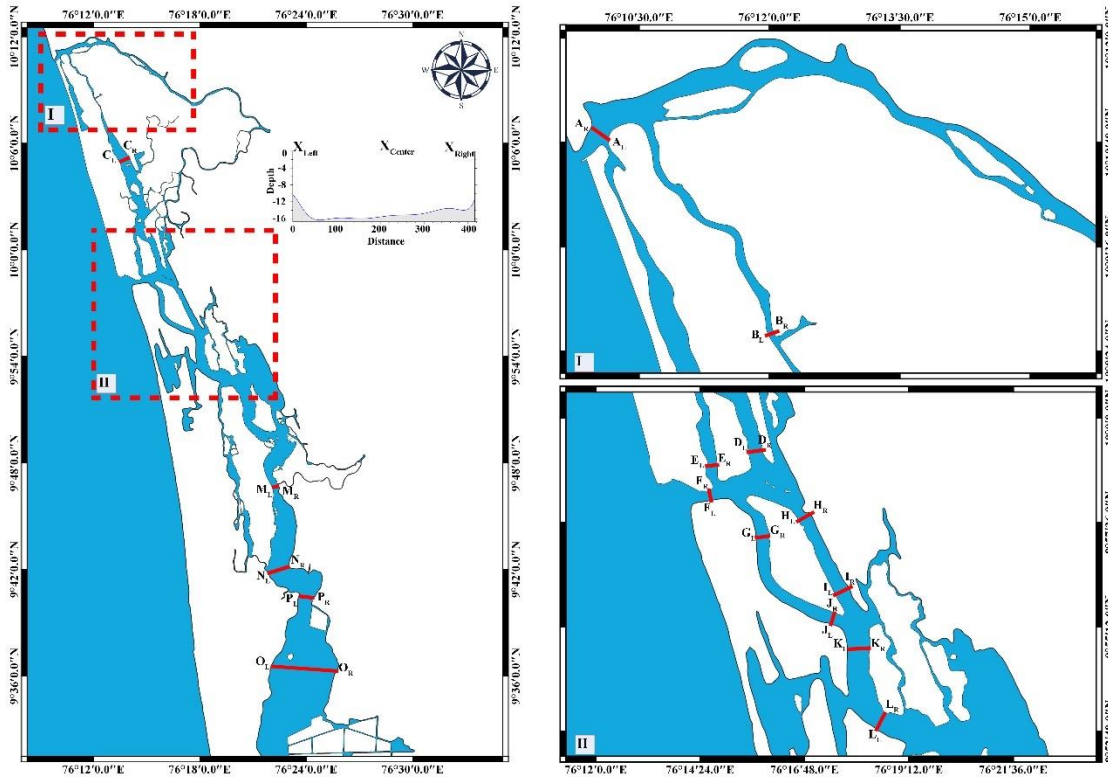


Fig. 1.3 Sixteen cross-sections (red line) perpendicular to the channel geometry are marked in the map and their respective depth-averaged velocities at three lateral stations (left, center and right of the channel) of VL are taken for the asymmetry analysis. The east and west shores of the lake are considered to be the left and right lateral stations of the channel cross-section except at A_L - A_R and F_L - F_R . The south and north shores of the A_L - A_R and F_L - F_R are considered to be left-right lateral station, as the boundary of the lake faces west-east directions.

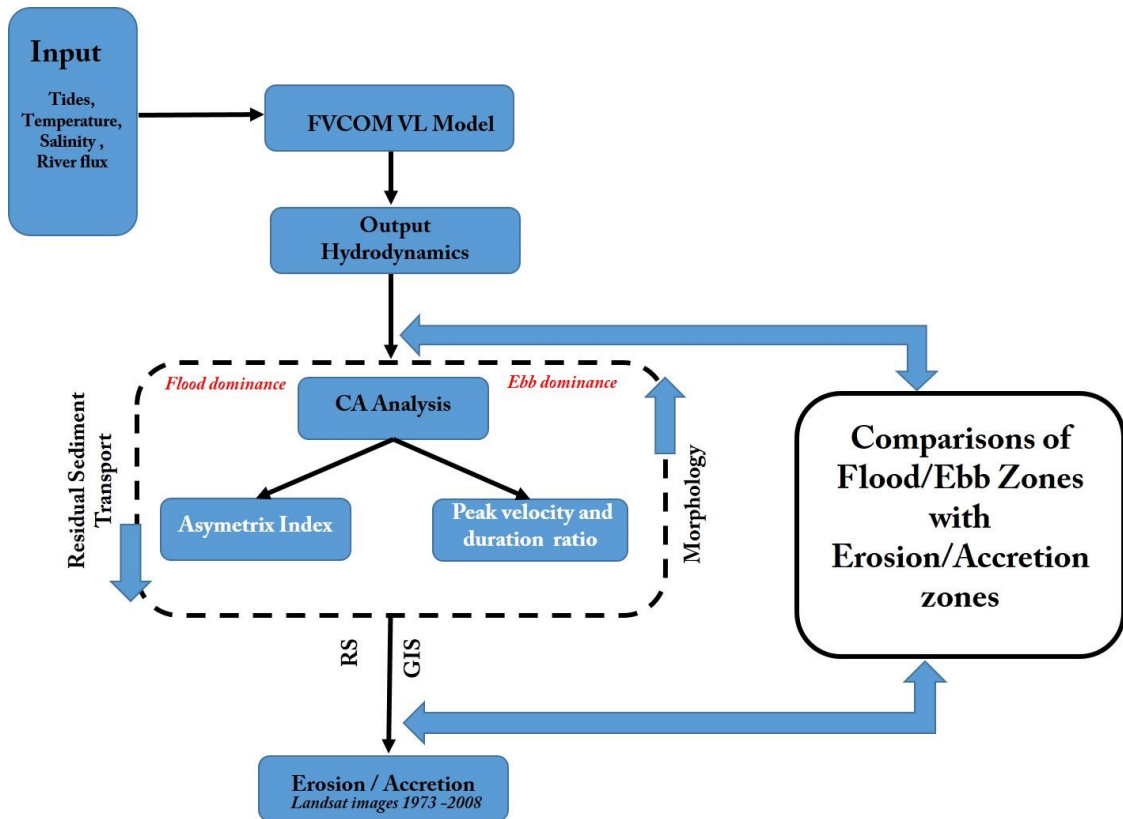


Fig. 2.1. Schematic diagram to understand the lateral variation of CA in VL and its implication on the morphological changes for the 3 decades.

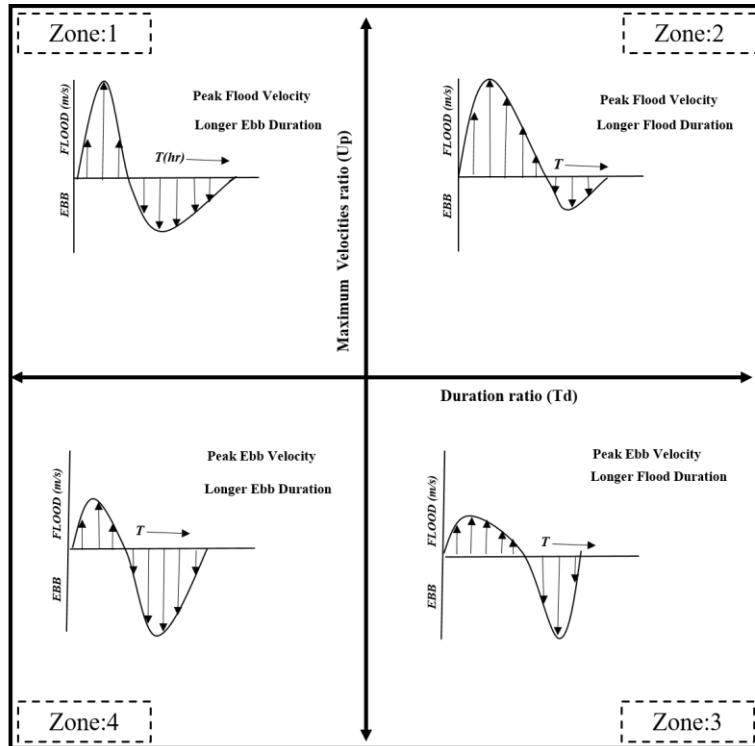


Fig. 2.2. The schematic diagram for representing four zones proposed by Davis and Brown (2010) in terms of CA.

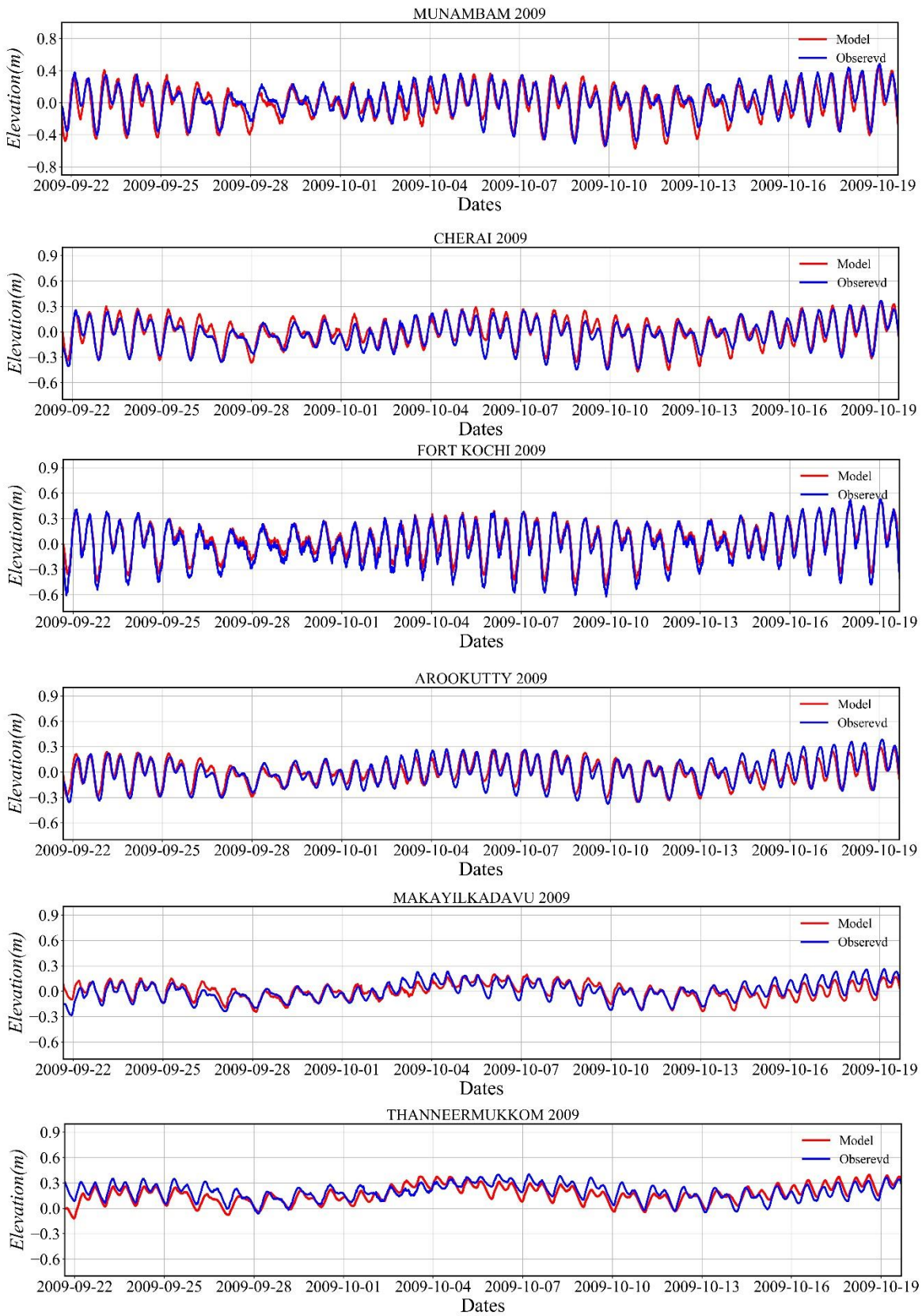


Fig. 3. Validation of tides at six locations of VL

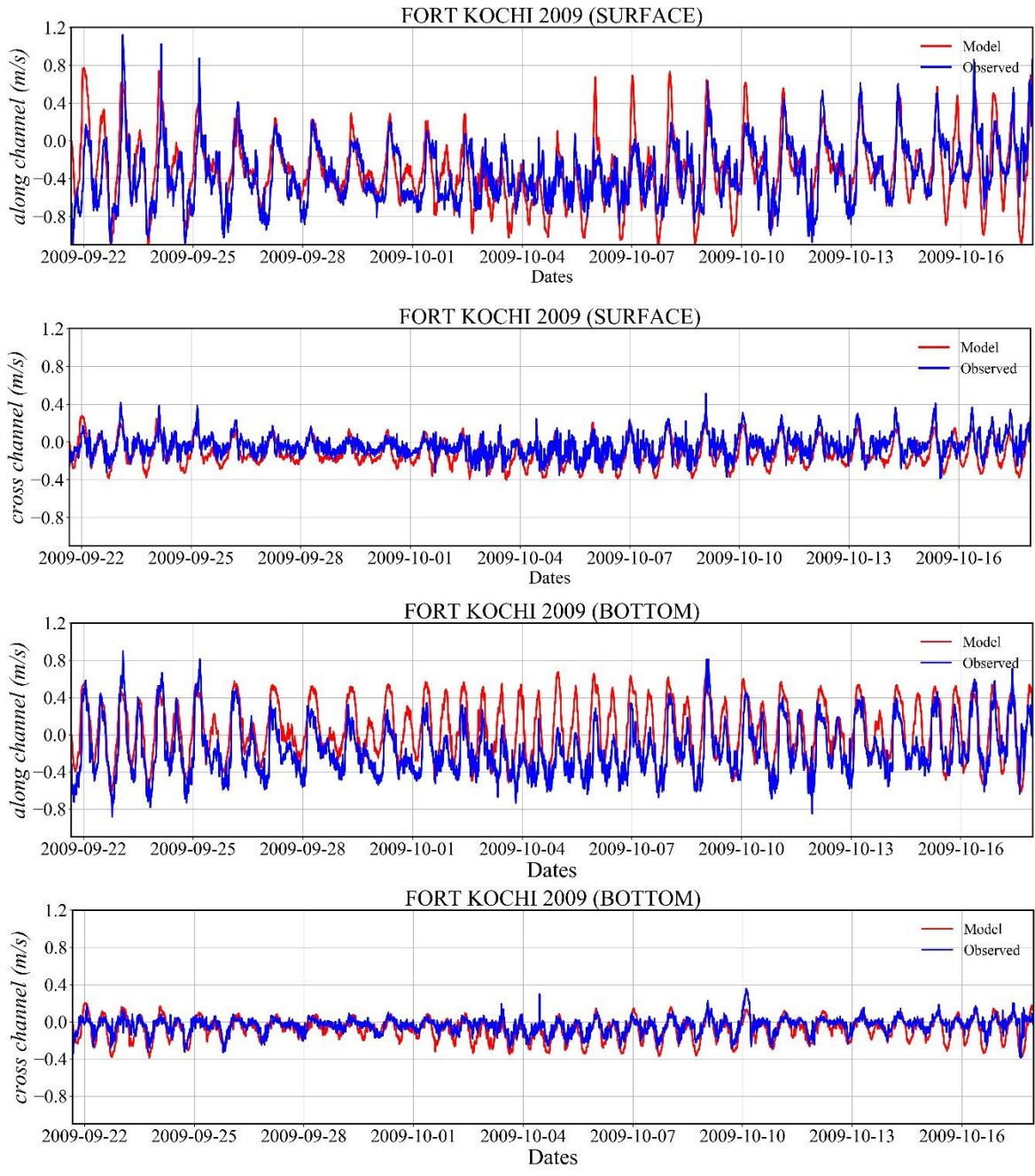


Fig. 4.1. Validation of surface and bottom currents at Fort Kochi (2009)

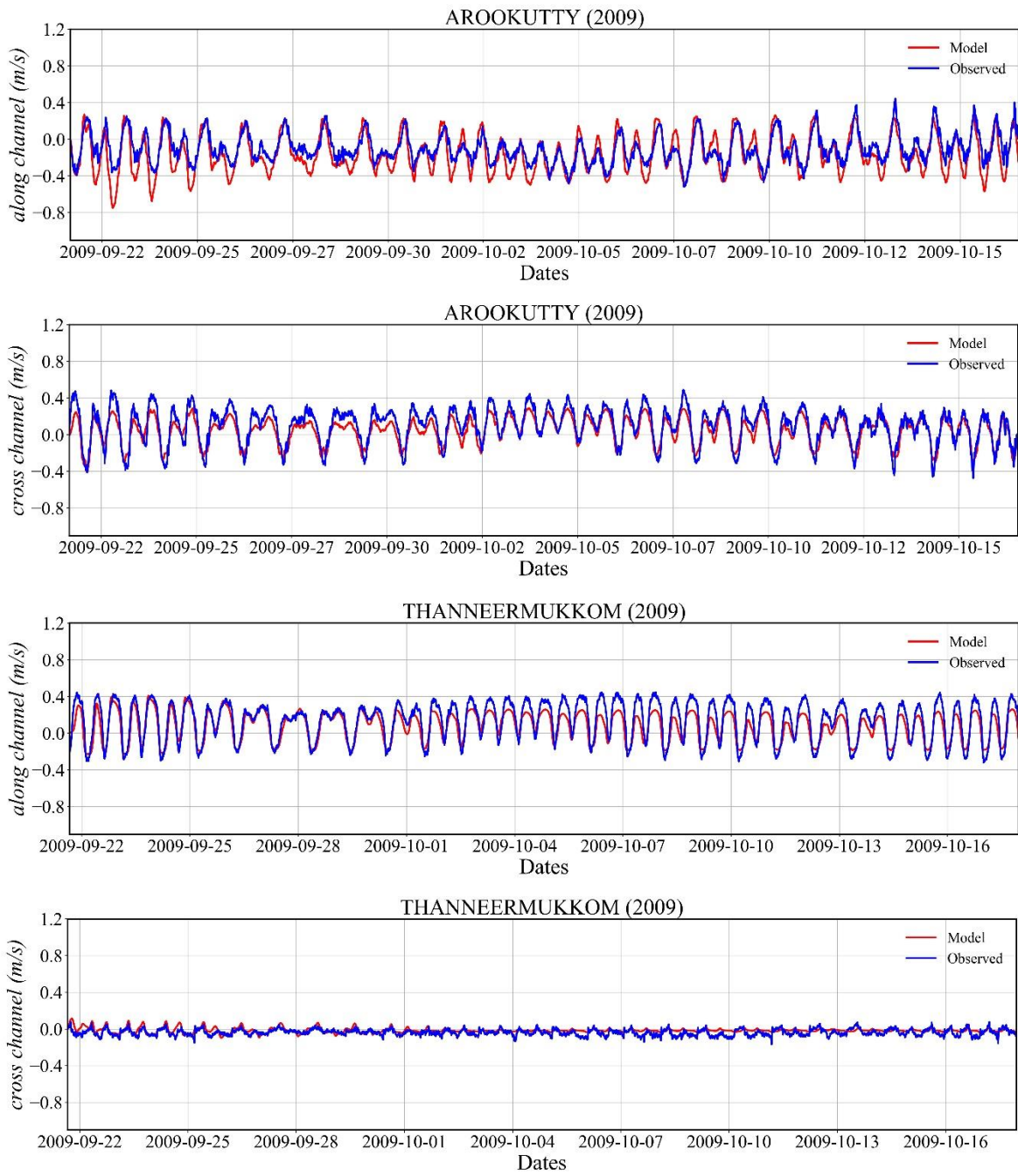


Fig. 4.2. Validation of surface currents at Arookutty and Thanneermukkom (2009)

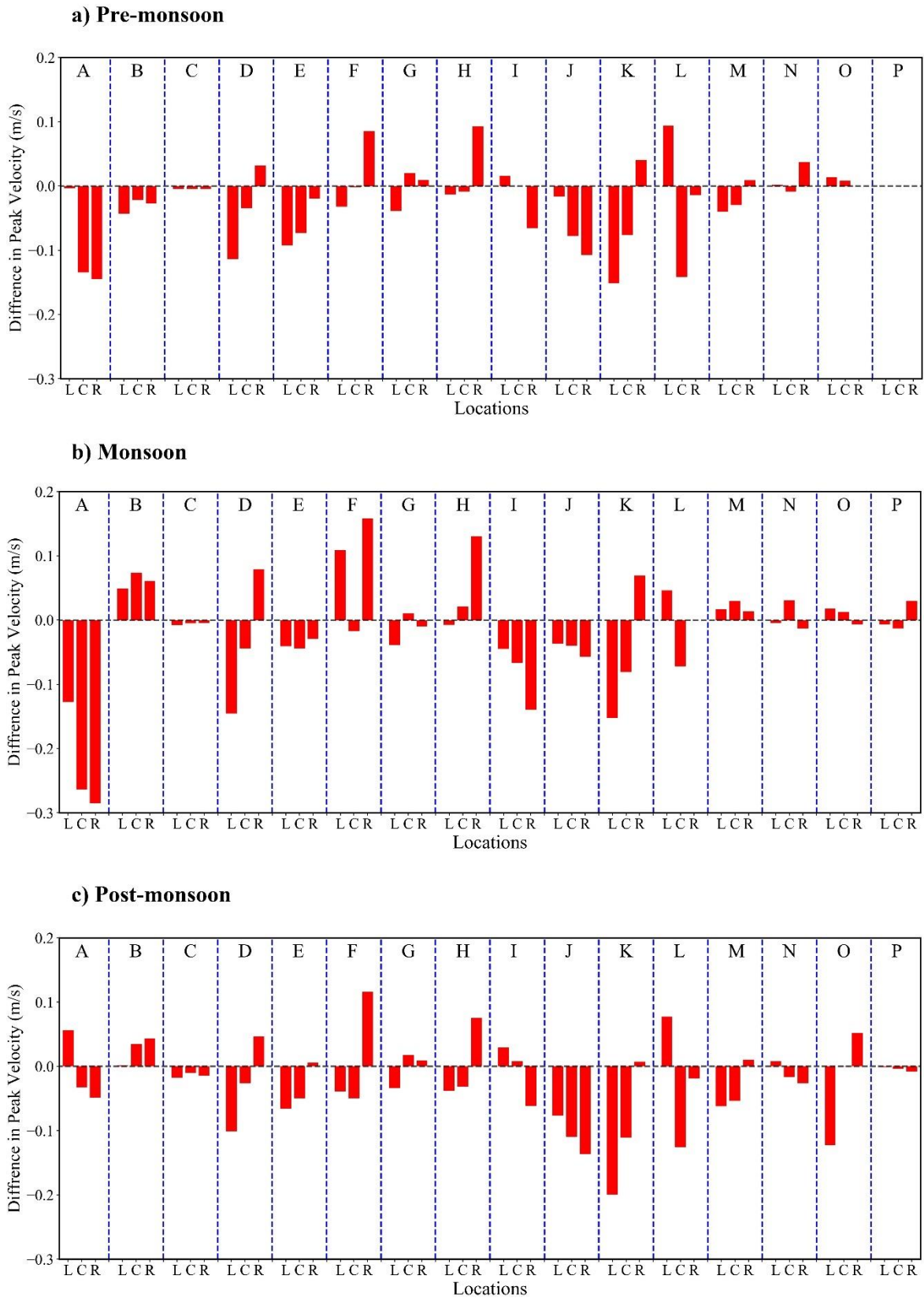


Fig. 5. Difference in the peak velocities along the 16-channel cross-section (A to P) during pre-monsoon (a), Monsoon (b) and post-monsoon (c). Positive value of the graph refers to the peak velocity was comparatively higher in flood than ebb and negative value refers to the peak velocity was comparatively higher in ebb than flood. 3 lateral stations of each channel cross-sections are marked inside of the blue dotted line (L-left, C-center, R-right)

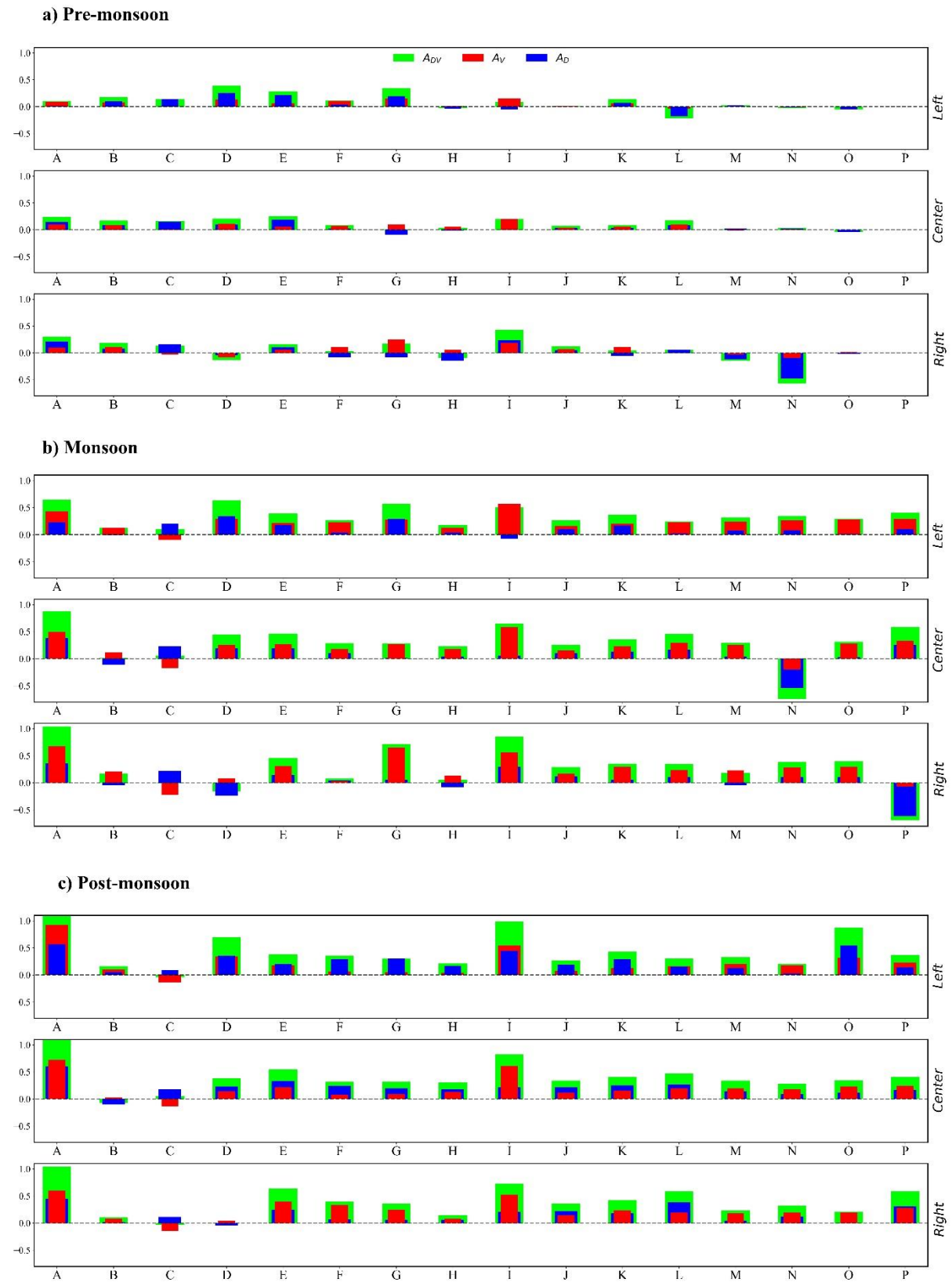


Fig. 6. Time duration asymmetry (A_D), Mean velocity asymmetry (A_V) and Asymmetry index (A_{IDV}) at left, center & right bank of the VL around 16 locations (A to P) during pre-monsoon (a), monsoon (b) and post-monsoon (c).

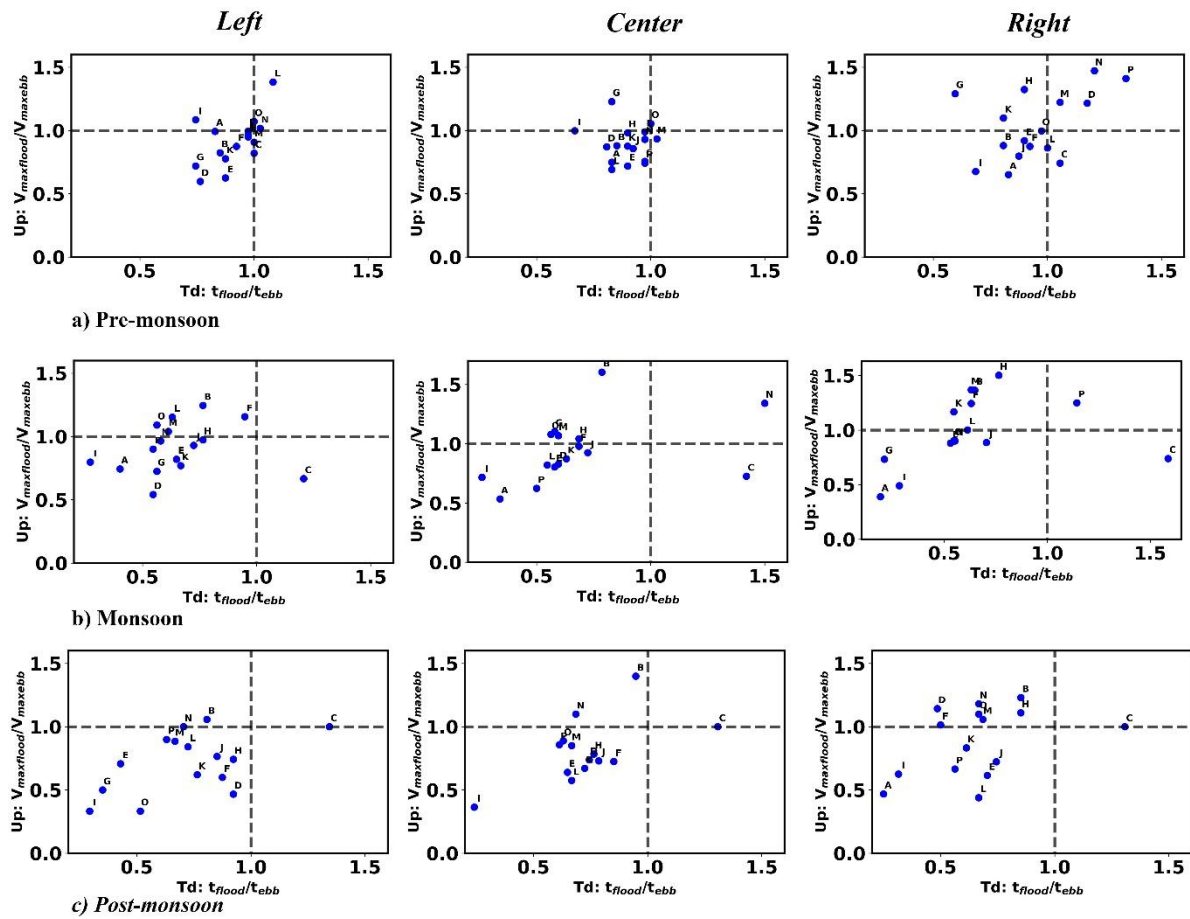


Fig. 7. Peak flow velocity ratio against the duration at left, center & right bank of the VL (four distinct zones for flood/ebb dominance are shown) during pre-monsoon (a), monsoon (b) and post-monsoon (c).

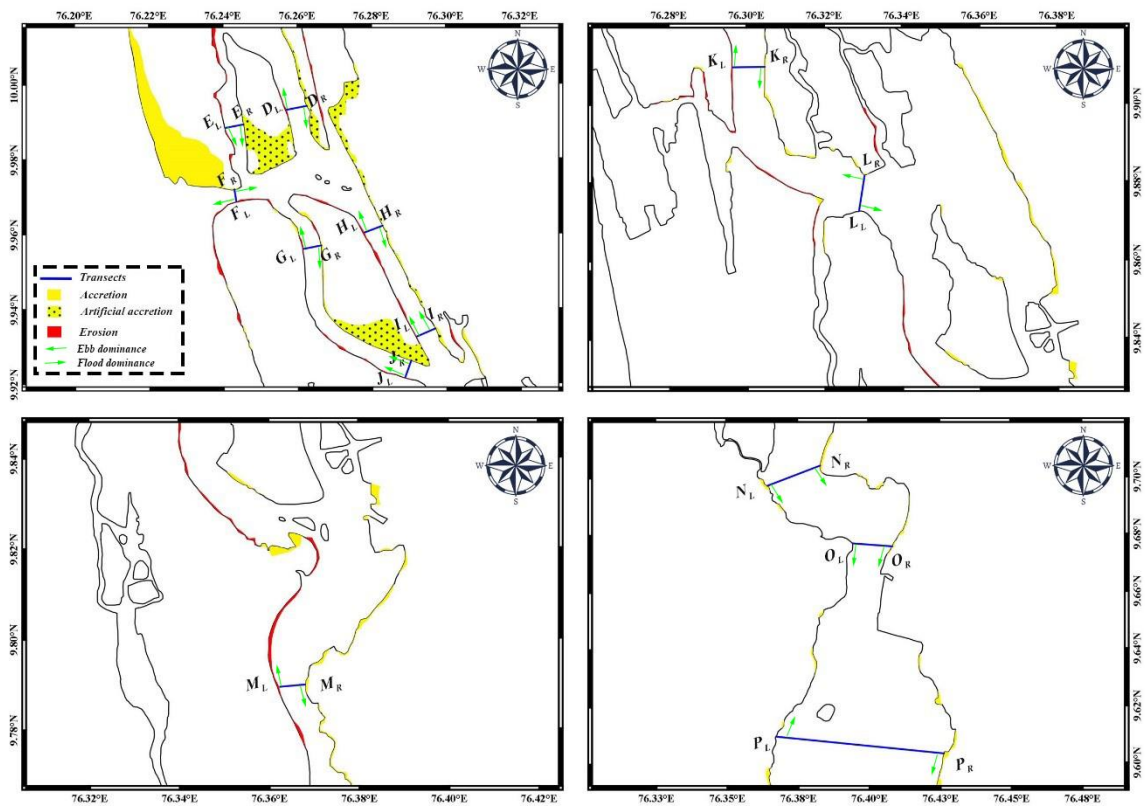


Fig. 8. Comparisons of flood/ebb dominance and accretion/ erosion zones in the VL (1973-2008).

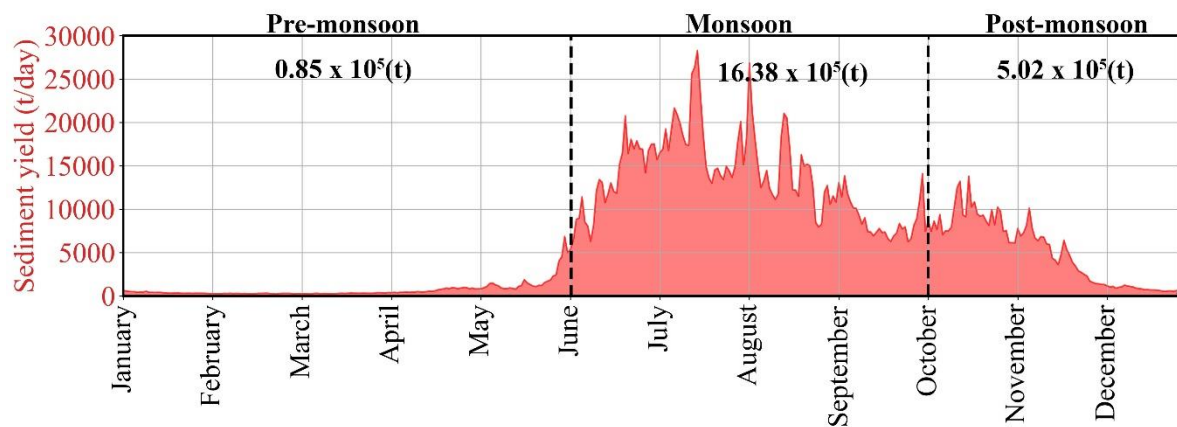


Fig.9. Climatological (2000-2016) daily sediment yield from the seven river basins to the VL. Daily sediment yield from the rivers are computed in the unit of tonnes/day. The average annual sediment yield is 22×10^5 t/yr. Seasonal transport of sediment yield to the VL is 0.85×10^5 tonnes in pre-monsoon (January-May), 16.38×10^5 tonnes in Monsoon (June-September) and 5.02×10^5 tonnes in post-monsoon (October-December).

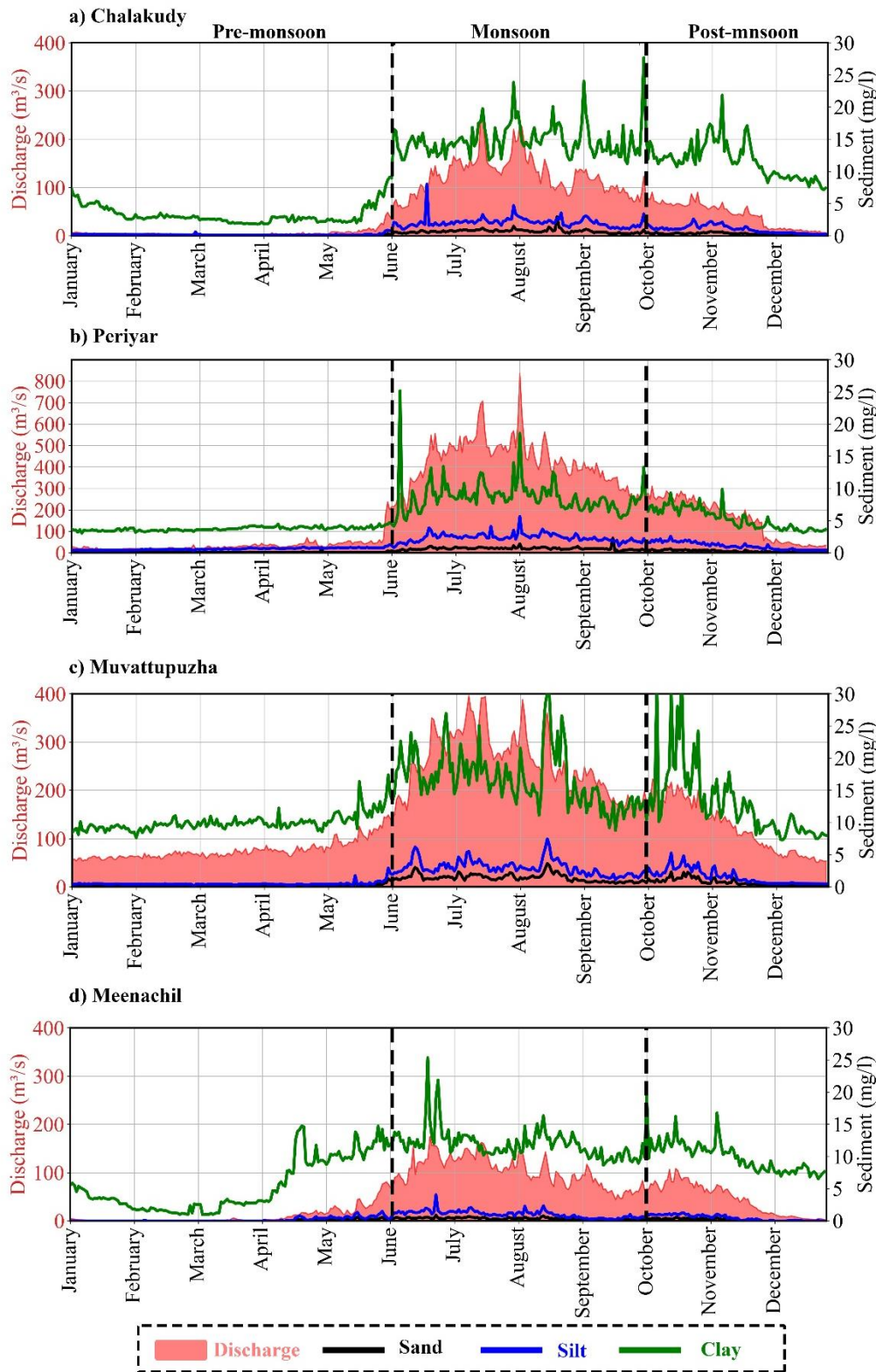


Fig.10.1 Climatological (2000-2016) daily river discharges and sediment concentration (Sand, Silt & Clay) of the river a) Chalakudy, b) Periyar, c) Muvattupuzha and d) Meenachil. Discharge and sediment data were obtained from the Central Water Commission, Government of India from the river gauge stations near VL (please refer the Fig 1.1 for the river gauge locations).

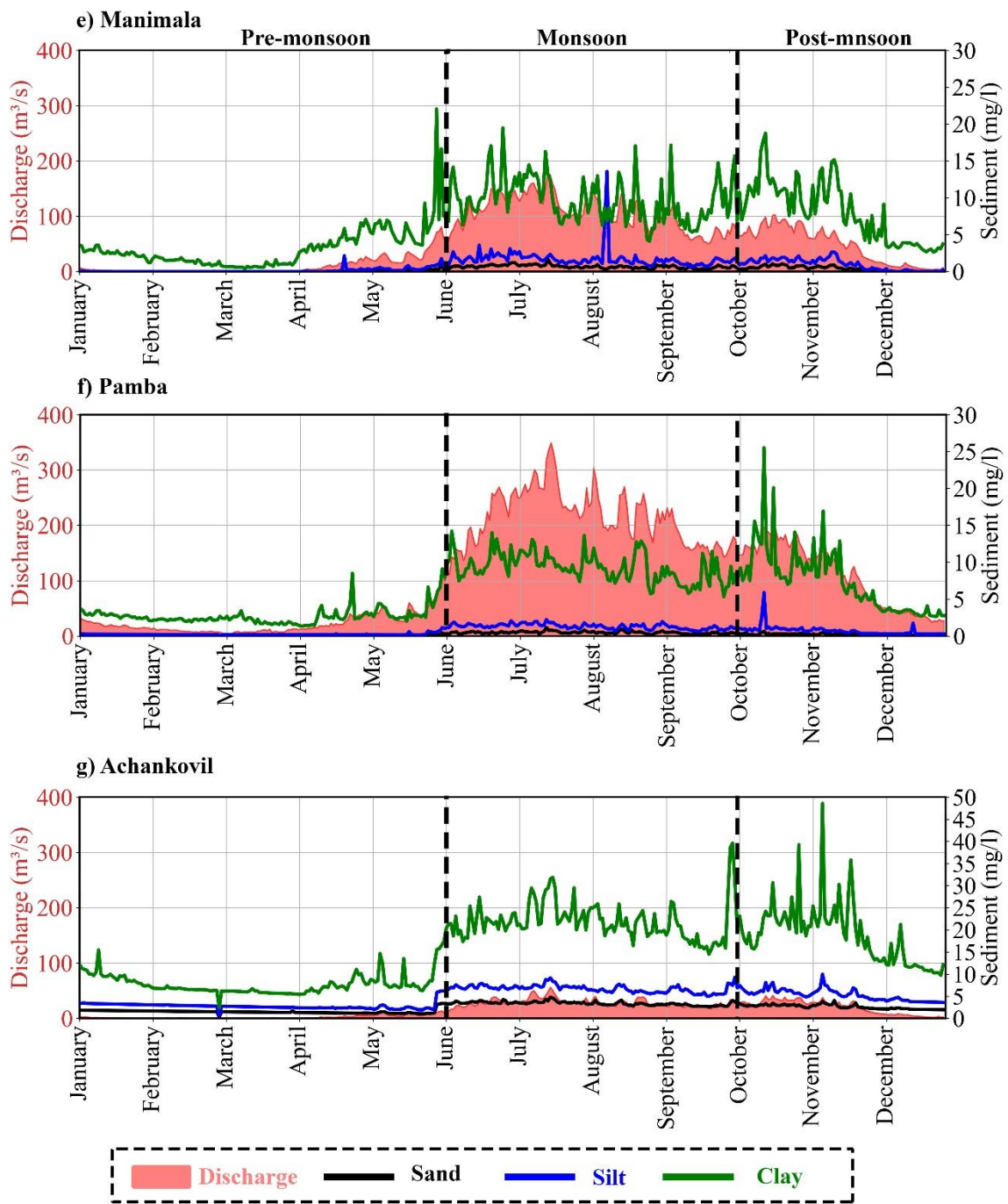


Fig.10.2 Climatological (2000-2016) daily river discharges and sediment concentration (Sand, Silt & Clay) of the river e) Manimala, f) Pamba, and f) Achankovil. Discharge and sediment data were obtained from the Central Water Commission, Government of India from the river Gauge stations near VL (please refer the Fig.1.1 for the river gauge locations).

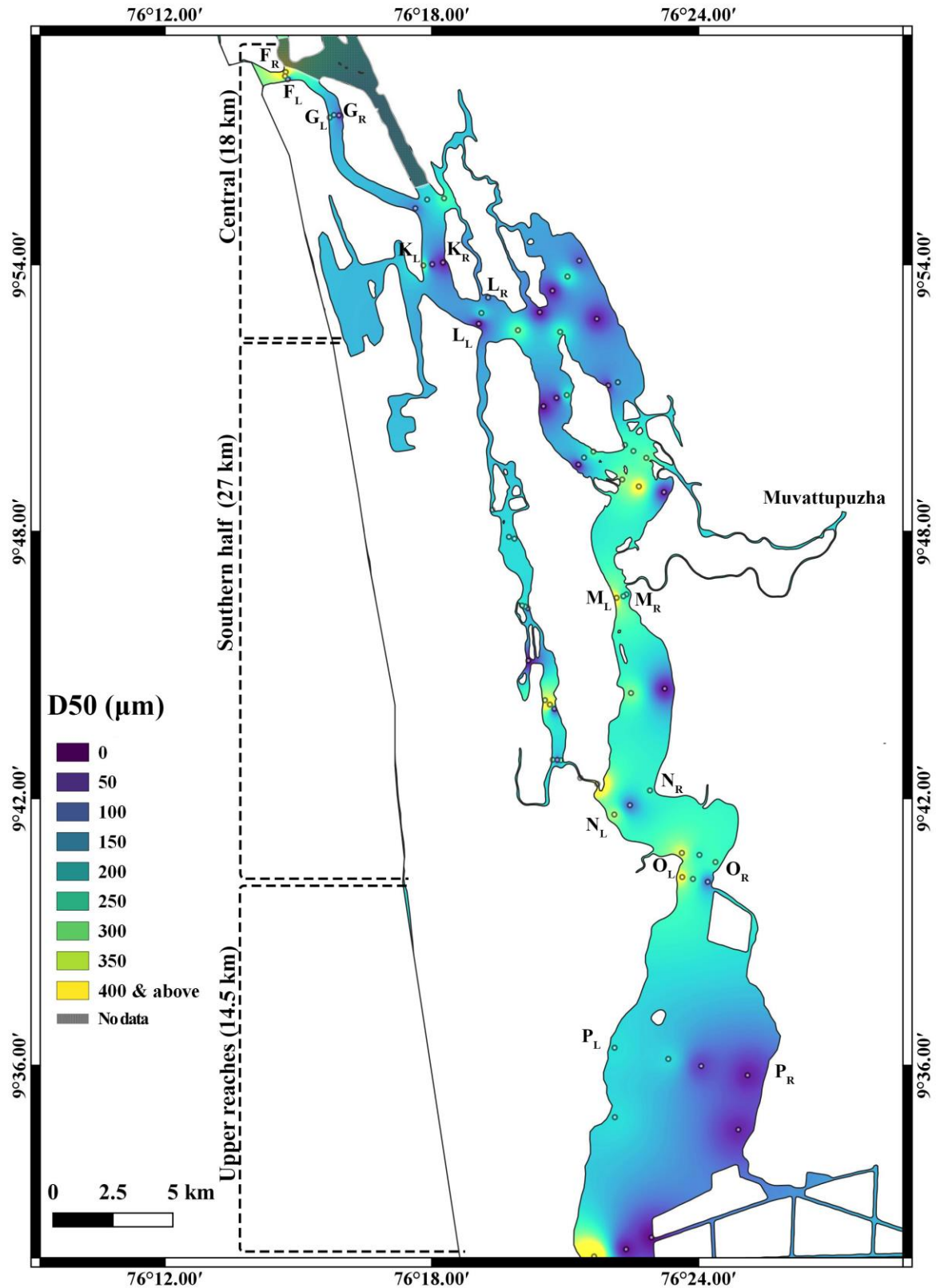


Fig. 11. Spatial distribution of sediment grain size of the VL. Seventy-five sediment samples collected along with the VL during the period of August 2013 for understanding the lateral (Left, Centre, Right) distribution of grain size (black-hollow circle on the figure represents the sampling locations around the VL). Among these, twenty-four sampling locations are exact points which we discussed for the CA analysis (F_L-F_R, G_L-G_R, K_L-K_R, L_L-L_R, M_L-M_R, N_L-N_R, O_L-O_R & P_L-P_R).

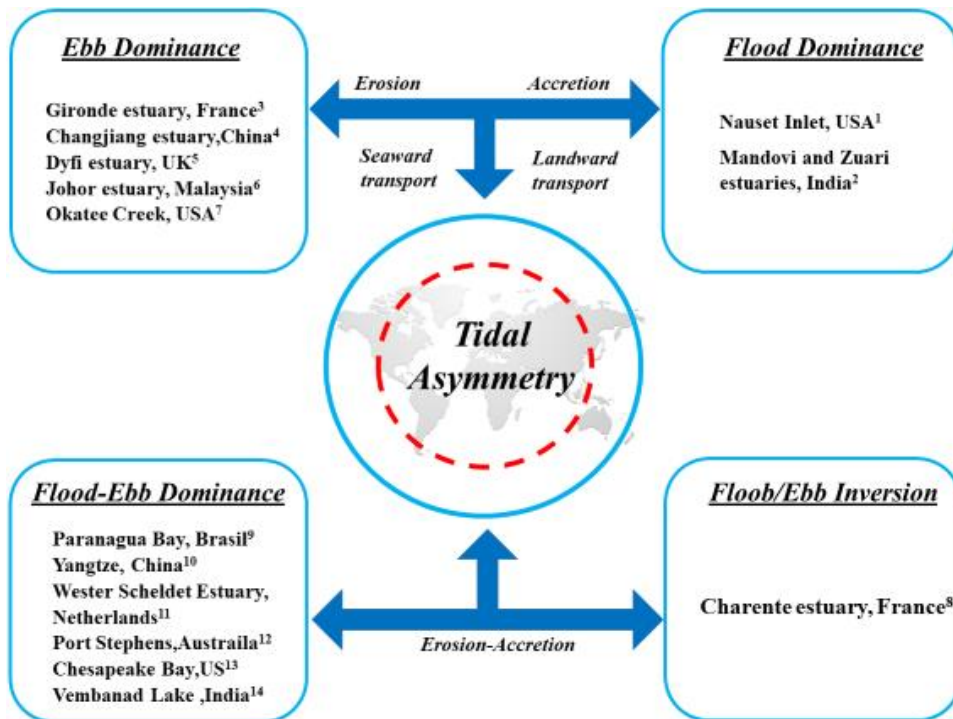


Fig. 12. A schematic diagram represents a comparison of the world estuaries (Thirteen different estuaries in the world) having flood/ebb dominance and its erosion/accretion process. The flood/ebb dominance of the estuaries are classified into four subdivisions (flood dominance, ebb dominance, flood-ebb dominance and flood/ebb inversion)

Tables:

Table 1

Statistical significance of predicted surface water elevation using Coefficient of Determination- R^2 , Root Mean Square Error and Index of agreement (d).

| Stations | RMS (m) | R^2 | Index of agreement |
|----------------|------------|-------|--------------------|
| Munambam | 0.06 | 0.89 | 0.94 |
| Cherai | 0.07 | 0.91 | 0.95 |
| Fortkochi | 0.07 | 0.99 | 0.97 |
| Arookutty | 0.07 | 0.89 | 0.94 |
| Makayilkadavu | 0.06 | 0.79 | 0.89 |
| Thanneermukkom | 0.07 | 0.75 | 0.85 |

Table 2

Statistical significance of predicted velocity using the Coefficient of Determination- R^2 , Root Mean Square Error and Index of agreement (d).

| Stations | Velocity Components | RMS (m) | R^2 | Index of agreement |
|------------------------|------------------------|------------|-------|-----------------------|
| Fortkochi (surface) | along- channel | 0.14 | 0.65 | 0.81 |
| | cross- channel | 0.14 | 0.68 | 0.75 |
| Fortkochi (Bottom) | along- channel | 0.15 | 0.64 | 0.80 |
| | cross- channel | 0.10 | 0.65 | 0.78 |
| Arookutty | along- channel | 0.12 | 0.81 | 0.95 |
| | cross- channel | 0.12 | 0.88 | 0.71 |
| Thaneermukkom | along- channel | 0.11 | 0.62 | 0.92 |
| | cross- channel | 0.04 | 0.81 | 0.60 |

Table 3

Comparison of the world estuaries (fourteen different estuaries in the world) having flood/ebb dominance and its erosion/accretion process

| Sl.No | Estuary | Dominance | Findings |
|-------|--|---------------------|---|
| 1 | Nauset Inlet, USA (Speerb and Aubrey, 1985) | Flood | Promotes Landward transport of coarse & near-bed materials |
| 2 | Mandovi and Zuari estuaries, India (Manoj et al., 2009) | Flood | Mandovi and Zuari estuaries are not frictionally dominated estuaries |
| 3 | Gironde estuary, France (Castaing and Allen, 1981) | Ebb | Net seaward flux is more than 100 times that measured during lean freshets |
| 4 | Changjiang estuary, China (Zhanhai et al., 2016) | Ebb | suspended sediment flux during the ebb was notably larger than during the flood |
| 5 | Dyfi estuary, UK (Brown and Davies, 2010) | Ebb | Flood/ebb dominance is attributable to the relative extent of the channels and sandbanks/flats |
| 6 | Johor estuary, Malaysia (Hasan et al., 2012) | Ebb | Ebb dominant sediment transport at narrow deep channel |
| 7 | Okatee Creek, USA | Ebb | Strongly stratified during ebb than the flood period. |
| 8 | Charente estuary, France (Toublanc et al., 2015) | Asymmetry inversion | Sediment accumulation in an intermediate zone between mouth and upstream |
| 9 | Paranagua Bay, Brazil (Mantovanelli et al., 2004) | Flood-Ebb | The nonlinear relationship between Velocities and SPM concentrations |
| 10 | Yangtze, China (Wang et al., 2008) | Flood-Ebb | volume and geometrical parameters of the channel have close relationships with the dynamic factors in the estuary |
| 11 | Western Scheldt Estuary, Netherlands (Nguyen et al., 2008) | Flood-Ebb | Large-scale residual circulation through ebb and flood channels |
| 12 | Port Stephens, Australia (Austin et al., 2009) | Flood-Ebb | Shallow wider region are flood dominated and narrower deeper channel are ebb dominant |
| 13 | Chesapeake Bay (Ahnert, 1960) | Flood-Ebb | The existence of separate paths are maintained for the peak ebb and flood velocities in Chesapeake bay |
| 14 | Vembanad Lake, India | Flood-Ebb | Peak flood/ebb velocity exceeds the ebb/flood having the tendency to the accretion/erosion process |